Review of Cooling Methods in Electric Vehicle Motors

Leng Wei
School of Mechanical and Automation Engineering Zhixing College of Hubei University, China
bobleng2015@sina.com

Abstract

Recently, there is an increasing number of electric vehicles for the purpose of protection of the environment and fossil fuels. An EV motor, such as PMSM, is the key component of an electric vehicle with its merits such as high-power density, compact structures, energy-efficient, high speed and so forth. The operation of an EV motor produces a large amount of heat, resulting in its high temperature. Without effective cooling methods, terrible problems will arise such as demagnetization of the motor, short circuit risk caused by winding insulation failure, and shortening the motor lifespan. Hence, it is essential to predict and monitor the motor temperature and develop thermal management. In this review, thermal analysis methods of the motor are described and compared in detail, which comprise FEA, CFD and LPTN. Furthermore, cooling methods constitute the main part of the review which are highlighted via simulations and experiments in different research. In the end, different cooling schemes in the cited papers are summarized in a table, and conclusion and outlook are made for the guidance of future work.

Key words EV motor; PMSM; Thermal management; Cooling method; CFD; FEA; LPTN; Active cooling method; Passive cooling method; Potting materials; Heat pipe; PCM; Fin; Hybrid cooling method.

1. Introduction

Traditional vehicles with an internal combustion engine (ICE) use gasoline which originates from petroleum as fuel. Burning gasoline is responsible for some serious problems, such as the impending depletion of fossil fuels and its damage to the environment, so it is urgent to take protective means. Escalating environmental contamination and dwindling fossil fuels prompt the automotive sector to pivot its attention to the electric vehicle (EV) market. EVs have gained prominence as a cleaner, more sustainable alternative to internal combustion engine vehicles, contributing to efforts to curb greenhouse gas emissions and combat climate change [1]. According to the development trend of vehicles, electric vehicles will completely replace the traditional ICE cars in the near future because of their lowest emissions and zero fuel consumption [2].

As the EV market expands, the mileage of an EV garners significant focus. An EV's travel distance is significantly influenced by severe driving conditions or the surrounding temperature. Enhancing the efficiency of EVs necessitates the implementation of an proper thermal management system. Apart from the battery, another core component of an EV is the electric motor which provides the driving force. The temperature rise of the electric motor is high during operation, which has negative impacts on the performance of an EV. Without effective cooling methods, overheating may result in some terrible consequences. Foremost, the motor needs additional power to adapt to conditions requiring high torque, such as climbing slopes or dealing with high or low ambient temperatures. It will lead to the motor overheating, causing its demagnetization and ultimately causing a decline in overall efficiency. In severe cases, the motor even needs to be replaced. Besides, overheating can also increase the internal resistance of the coil winding, intensifying heating. Furthermore, overheating may cause the insulation layer of the wire to melt, resulting in short circuits and even motor winding burning down. Additionally, EV components are exposed to diverse operational and environmental conditions, including rapid acceleration, prolonged high-load operation, and extreme ambient temperatures [3]. These factors exacerbate the thermal loads on components and demand adaptive cooling strategies to ensure consistent performance [4]. Consequently, predicting and preventing an EV motor's excessive temperature increase during the design phase through thermal simulation techniques is crucial. Researchers are focusing on enhancing these vehicles' efficiency through the integration of a proficient thermal management system.

In most cases, the cooling methods can be mainly classified into two types - the passive one and the active one. The passive cooling methods comprise natural air cooling, such as the optimization of design for fins, heat pipes (HPs), phase change materials (PCM), etc. The active cooling methods comprise forced air cooling, liquid cooling, etc. Air cooling,

characterized by convective heat transfer, is cost effective and straightforward to implement [4]. However, its capacity to dissipate heat is often inadequate for high-power-density applications. In contrast, liquid cooling systems, which utilize water or oil-based coolants, offer significantly higher thermal performance [4]. Liquid cooling is particularly effective in dissipating heat from compact, high energy-density systems, making it suitable for modern EVs [5]. In recent years, it has been proved that hybrid cooling methods are much more effective than a single one. For instance, oil-air mixed cooling and phase change material coupled with liquid cooling. This review article will provide a detailed description of the following sections.

In the realm of electric vehicles, the top three favored motors include the permanent magnet synchronous motor (PMSM), induction motor (IM), and switched reluctance motor (SRM). In Ref. [6], A. M. Lulhe et al. lists the comparison of these three types of motors, concluding that PMSM is more advantageous than IM and SRM, so PMSM is most popular among them. The advantages of PMSM lie in its elevated power density, high energy conversion efficacy, light weight, low-speed and high torque characteristics. A motor's function is to convert electrical energy to mechanical energy to perform useful work [7]. In this process, an EV motor will generate a large amount of heat due to motor losses.

2. Overview of Heating Mechanism of PMSM

From Fig.1, main sources of heat generated are motor power losses composed of iron losses, copper losses, mechanical losses and stray losses. Main heating components of PMSM are stator windings, a stator core and a rotor core.

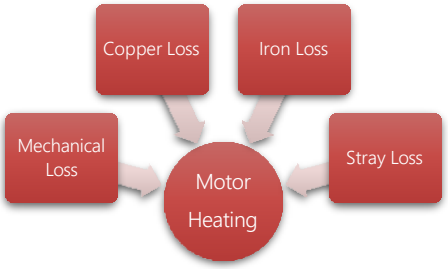

Fig.1 Main Sources of Heat

2.1 Copper Losses

Copper losses in electric motors are a fundamental source of energy dissipation arising from the electrical resistance of the copper windings in motor coils [8]. As electrical current passes through stator's copper windings of the motor, the inherent resistance of copper conductors converts electrical energy into heat that can be predicted via Joule's Law. And this heat can be calculated with Equation (1) shown below:

$$QCu = I^2Rt \quad (1)$$

From Equation (1), copper losses are directly proportional to the square of the current I am flowing through copper windings, the resistance R of copper windings and working time t. Higher current levels result in increased copper losses because of the elevated power dissipation caused by the greater flow of electrical energy through the resistive conductors [9]. Additionally, copper losses contribute to heat build-up within the motor windings, leading to elevated temperatures [9]. Furthermore, electrical current passing through windings is responsible for voltage drop, influencing the voltage available to drive the load. This voltage drop can do harm to efficiency and performance of PMSM.

In winding copper losses, over 60% of the motor's total heat is due to the Joule heat produced as current flows through the stator windings, constituting the bulk.

2.2 Iron Losses

Iron losses are another significant source of energy dissipation in PMSM which is also known as core losses or magnetic losses and arise on the magnetic core of a motor. Iron losses mainly comprise hysteresis loss and the eddy loss.

Hysteresis Loss The energy loss caused by hysteresis in ferromagnetic materials during alternating magnetization is called hysteresis loss, which arises due to dynamic magnetization and demagnetization processes of the core material during motor operation. Hysteresis loss can be calculated by Stamets empirical formula shown in Equation (2) below:

$$Ph = \eta \cdot f \cdot Bnmax \cdot V \quad (2)$$

(η—the material loss coefficient related to the hysteresis characteristics of the material and reflects the difficulty of magnetic domain flipping inside the material; f—the frequency of alternating magnetic field, which is the number of times the direction of the magnetic field changes per second; Bnmax—the maximum magnetic flux density, which is the maximum magnetic induction intensity achieved by the material in an alternating magnetic field; V—the effective working volume of magnetic materials)

Eddy Loss Eddy loss is caused by eddy current. It is known that ferromagnetic materials can not only conduct magnetism but also conduct electricity. When there is alternating current flowing through the coil, the magnetic flux it generates is also alternating. Therefore, induced electromotive force and induced current will be generated inside the iron core. This induced current is named eddy current resulting in Joule heat because it forms a vortex in a plane perpendicular to the direction of magnetic flux. Eddy loss can be calculated by Equation (3) below:

$$Pe = Ke \cdot (f \cdot Bmax \cdot t)2 \cdot V \tag{3}$$

(Ke—eddy current loss coefficient, related to material properties; t—the thickness of material)

And the meanings of the other parameters are the same as that of Equation (2).

In brief, as for stator iron losses, the alternating magnetic field is responsible for eddy current losses and hysteresis losses inside the iron core, accounting for about 20% of the total heat generation of the motor. The energy lost in the form of heat in the core material is wasted electrical power, which decreases the overall motor efficiency of the motor [10]. Iron losses have significant impacts on the performance and efficiency of electric motors. All in all, iron losses can be calculated by Equation (4):

$$Piron = Ph + Pe \tag{4}$$

2.3 Mechanical Losses

Mechanical losses are mainly caused by the heat generated by friction between different components of an electric motor during the operation, which directly affects EV's efficiency, constituting roughly 10% of the total heat generation. It mainly consists of the bearing loss resulted from friction between bearings and the track or lubricant during high-speed rotation, and the windage loss resulted from the turbulence generated by friction between the rotor surface and air. The mechanical losses can be calculated as Equation (5):

$$Pmech = Pbearing + Pwindage = a_1\omega + a_2\omega_2 + a_3\omega_3 \tag{5}$$

($Pbearing$—bearing losses; $Pwindage$—windage losses; ω—speed; a_1, a_2, a_3—coefficients) [11]

2.4 Stray Losses

Stray losses stem from stray no-load losses resulted from alterations in the main magnetic flux and stray load losses resulted from leakage magnetic flux. The magnitude of these losses fluctuates based on the square of the load current, resulting from leakage flux caused by load currents in the laminations, constituting 4~5% of the overall losses. In spite of its small percentage, stray losses still play the devil with the efficiency and the performance of an electric motor. These losses also contribute to heat buildup within the motor, potentially leading to thermal degradation of motor components and impaired motor performance and reliability over time [12].

3. Overview of Thermal Analysis Methods for Electric Motors

Because temperature has a huge impact on different components—such as permanent magnet (PM), stator windings—of an EV motor, thermal analysis is thus required to ensure that a prototype motor will be able to sustain its theorized performance [13]. Techniques for analysis of motor heat include FEA, CFD, and LPTN, which are short for finite element analysis, computational fluid dynamics and lumped parameter thermal network respectively. Each of these methods has their own characteristics.

3.1 FEA & CFD

A popular and traditional method is that of finite element analysis (FEA) modelling of heat transfer through a complex mesh at the cost of computation time [14]. This problem compounds upon itself when tractions motor designs are altered early in the design process, since even minor geometric alterations necessitate the complete reconstruction of the mesh [14]. Computational fluid dynamics (CFD) is a system analysis involving fluid flow, heat transfer and some associated phenomena such as by means of computer-based simulation chemical reactions [15].

There is a close relationship between motor heating and motor electromagnetic field, so research always focuses on both of the electromagnetic analysis and thermal analysis. A simulation software called ANSYS is used for FEA and CFD. Electromagnetic analysis is conducted by ANSYS Maxwell, while thermal analysis by ANSYS Fluent.

In Ref. [16], O. Ustun et al. make a detailed electromagnetic FEA analysis for designing and manufacturing an electric motor. They create an electromagnetic FEA 2D model (in Fig.2) and 3D model (in Fig.3) of an electric motor and make electromagnetic analysis with ANSYS Maxwell software to verify the motor calculations, acquiring the torque-time graph and the winding currents-time graph. By ANSYS Maxwell, it is shown in Fig.4 that they obtain a flux line field map with a time step 5 ms, indicating that magnets provide sufficient magnetic flux density to generate magnetic field in air gap and produce switching effects on the excitation. They also obtain magnetic flux density graph (in Fig.5), showing that laminated steel is not saturated. In addition, ANSYS Fluent software is used for CFD. In this study, water cooling with serpentine-type passages is adopted for thermal management. To find out average temperatures of stator windings, they arrange 4 different flow rates, i.e., 4L/min, 8L/min, 12L/min and 16L/min. The simulation results can be seen in Fig.6 that the water-cooling system is maintaining the operational temperature around 81°C, below 90°C—the targeted temperature.

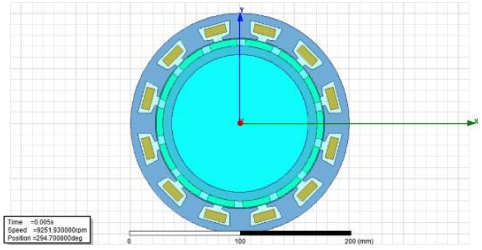

Fig.2 Motor 2D FEA Model[16]

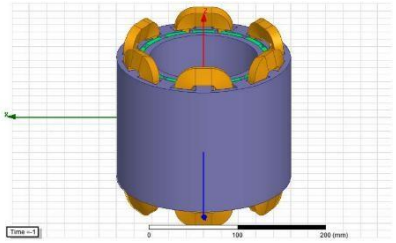

Fig.3 Motor 3D FEA Model[16]

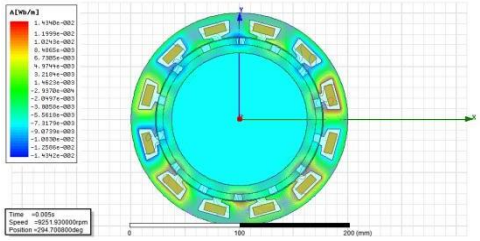

Fig.4 Flux Line Field Graph[16]

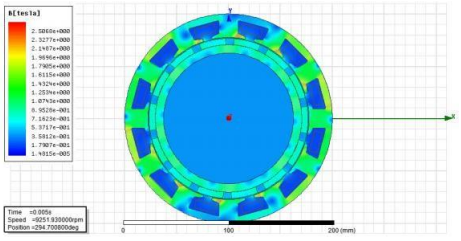

Fig.5 Magnetic Flux Density Graph[16]

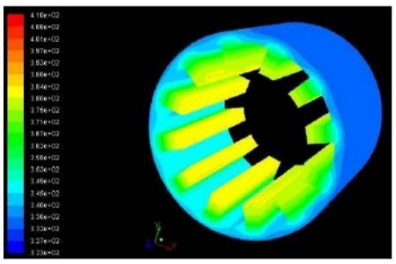

Fig.6 Distribution of temperatures in stator of serpentine type with water flow rate of 8 L/min [16]

In Ref. [17], Ye Li et al. design an oil-water composite cooling system. They also use ANSYS Maxwell software to simulate and calculate electromagnetic losses of PMSM. The electromagnetic simulation results of the motor are displayed in Table 1. Fig.7 and Fig.8 illustrate the distribution of magnetic field lines and the magnetic density throughout the loading process. Furthermore, they use ANSYS Fluent software for mesh generation and grid independence verification, showing the division of the boundary layer of the flow channel (in Fig.9). In addition, they propose 3 designs of cooling structures to cool oil using water cooling devices inside the motor casing. The comparison and analysis of temperature distributions of 3 designs are conducted by ANSYS Fluent. Finally, they provide suggestions for their practical applications according to the simulation and analysis results.

Table 1 Results [17]

Parameter	Value	Parameter	Value
Average phase current (A)	474.1	Bus voltage (V)	450
Average torque (N·m)	118.8	Copper loss (W)	792
Iron loss (W)	7893	Average current density (A/mm²)	10.8
Maximum current density (A/mm²)	29.05	Speed (rpm)	22000

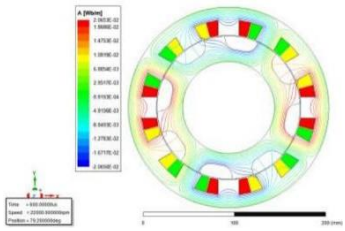

Fig.7 Magnetic Field Lines during Load Operation[17]

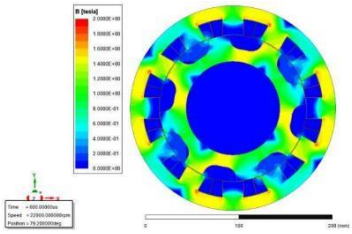

Fig.8 Magnetic Density Distributionduring Load Operation[17]

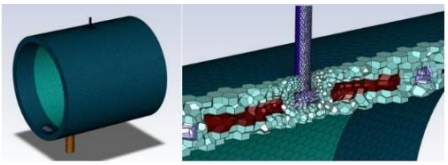

Fig.9 Schematic Diagram of the Grid [17]

In thermal analysis of an electric motor, FEA has high accuracy, but it is time-consuming; while CFD is feasible, it is resource-consuming. Rather than depending on these complex and time-consuming models, a different form of heat analysis can be implemented through the lumped parameter thermal network (LPTN), of which the analysis time is the shortest among the three methods.

3.2 LPTN

Lumped Parameter Thermal Network (LPTN) model is a temperature prediction tool for the motors, which can provide temperature results much faster under dynamic driving conditions [18]. Compared to FEA and CFD, LPTN stands out as a more apt technique for temperature prediction.

3.2.1 A Brief Overview of LPTN's Principle

In the thermal analysis of a product such as an electric motor, it is not always necessary to pay much attention to the detailed distribution of temperature in a certain component, but rather to the overall temperature of all components and the heat transfer between different components. In response to this demand, LPTN is a tool which can simplify objects and quickly calculate while ensuring a certain level of computational accuracy.

As is shown in Fig.10 a, an object is composed of 9 parts, each of which is respectively named as ***Part a~i.*** All of the physical properties of each part with a certain volume can be aggregated into one node, including mass, volume, temperature, etc. Therefore, the overall temperature of each part can be reflected by the temperature of one node. For instance, T_e represents the temperature of the Node e, reflecting the overall temperature of ***Part e***. Any two nodes are connected by a heat transfer pathway (black lines in Fig.10 b). And heat transfer includes heat convection, heat conduction and heat radiation. Thus, these pathways form a network. In each pathway, there is a thermal resistance used to reflect the difficulty of heat transfer between two nodes. For instance, R_{ae} is the thermal resistance that reflects the difficulty of heat transfer between ***Node a*** and ***Node e***. These nodes, heat transfer pathways and thermal resistances together form the LPTN. In short, in the LPTN model, each component of the motor is treated as a node where the average properties of a particular component are lumped. LPTN is analogous to an electric circuit, in which a thermal resistance is similar to an electric resistance, heat transfer pathways are similar to wires, and the temperature difference can be compared to the voltage. The intersection of two wires in an electric circuit is also called a node. The heat transfer between different nodes and within

the thermal resistance in LPTN is like the current flowing between different nodes and within the resistance in an electric circuit.

In addition, this model assumes a uniform temperature distribution, which may introduce errors in asymmetric structures.

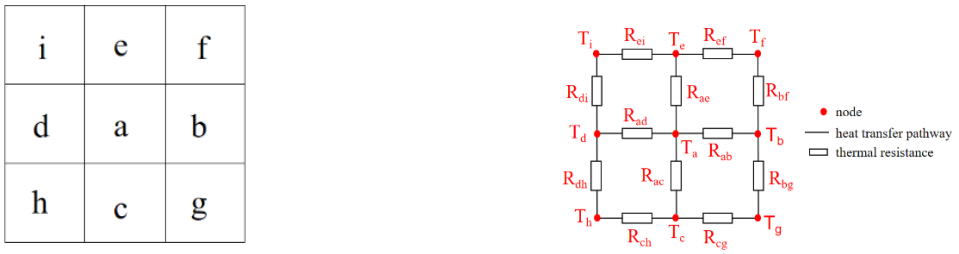

a) b)

Fig.10 Simple heat transfer system and its corresponding thermal network

3.2.2 Application of LPTN in an Electric Motor

In Ref. [11], So-Yeon Im *et al.* study thermal modeling of a hybrid electric vehicle motor. In this study, the cooling method of the motor is direct oil cooling by automatic transmission fluid (ATF). From Fig.11, LPTN models the motor's heat dissipation to predict temperatures of different motor components, such as the stator yoke, end windings, stator windings and PMs. In Fig.11, heat dissipation can be calculated by Equation (6) below:

$$QATF = hATFA(Tcomponent - TATF) \tag{6}$$

($\boldsymbol{h_{ATF}}$ —the convective heat transfer coefficient (HTC) by ATF; $\boldsymbol{T_{ATF}}$ —the temperature of the ATF; $\boldsymbol{T_{component}}$ —the temperature of the motor's particular parts in contact with the ATF.) The contact thermal resistance between the rotor core and shaft, between the PM and the rotor core, and between the housing and the stator yoke can be calculated by Equation (7):

$$Rcont = \frac{1}{hcontA} \tag{7}$$

($\boldsymbol{h_{cont}}$—the boundary film coefficient of contact heat transfer; $\boldsymbol{A}$—the surface area in contact)

The convective thermal resistance between the housing and ambient, between the air gap and the stator teeth/rotor core, and between the end cap air and each component can be calculated by Equation (8):

$$Rconv = \frac{1}{hconvA} \tag{8}$$

($\boldsymbol{h_{conv}}$—the convective HTC).

The convective HTC of the air gap can be calculated by Equation (9):

$$hgap = \frac{kNu}{lgap} \tag{9}$$

($\boldsymbol{Nu}$—the Nusselt number; $\boldsymbol{k}$—the fluid conductivity; $\boldsymbol{l_{gap}}$—the length of air gap)

To enhance the reliability of LPTN's temperature prediction with direct oil cooling, the convective HTCs of ATF which are determined by correlation with results of the experiment should be optimized by the kringing surrogate model, which is a functional relationship between parameters and responses and has low computation time and good accuracy. The design parameters consist of a mix of HTCs of ATF, and the experiment design is conducted based on them. Furthermore, the root means square error (RMSE) of the predicted temperature and the experimentally measured temperature, and the difference between the two saturated temperatures (DST) are reflected in responses. RMSE and DST can report the accuracy of temperature prediction. The function with multiple objectives optimized through kriging substitution model aims to minimize the difference between predicted temperature and measured temperature. The comparison results of the predicted temperature and the measured temperature show that the direct oil-cooled LPTN which reflects the evaluated HTCs has high prediction accuracy due to the fact that the RMSEs and DSTs for each component are smaller than 8% and 8℃ respectively. One of the results of comparison is shown in Fig.12.

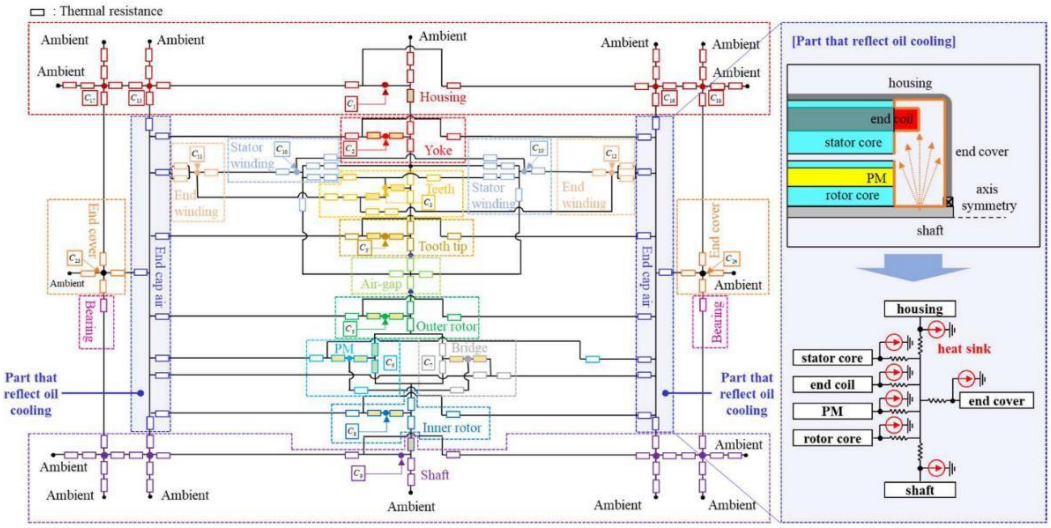

Fig.11 Configuration of direct oil-cooled LPTN[11]

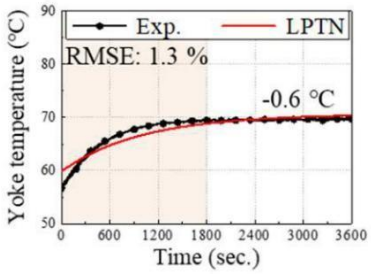

Fig.12 Comparison of the experiment's measured temperature and the LPTN's predicted temperature

(Load condition of 1000 rpm and 40 N·m) [11]

In Ref. [18], Mohammed Towhidi *et al.* propose a modified LPTN model (in Fig.13) for traction IM application. Motor losses cause the motor to produce heat and are used as inputs for the model. The model will provide temperature results for different motor components as outputs as soon as the loss inputs are given and the thermal resistances and capacitances are set up. In Fig.13, Core losses, stator winding losses and rotor copper losses are respectively connected to stator thermal block, winding thermal block and rotor thermal block. One pathway marked with red line in this figure is taken for example. Heat occurs from rotor copper losses, passes through the rotor core through the process of thermal conduction, then passes through the air gap in the form of thermal convection, and finally reaches the stator winding, reflecting the corresponding temperature result.

In their research, this LPTN model is used to study the thermal behavior of an induction motor (IM) under different torque-speed conditions with varying liquid coolant flow rates, based on the fact that the motor temperature is highly related to torque and speed. They use LPTN to obtain several simulation results for the motor's component temperature under high torque-low speed and low torque-high speed conditions, finding that the loss value gets saturated as soon as the torque reaches 36 N·m (rated value). Furthermore, by this LPTN model, they determine the optimal flow rate of liquid coolant(water-glycol) at different torque-speed conditions. Fig.14 is one of the temperature results, showing that 5 lpm is the optimal flow rate of liquid coolant at motor conditions of 4.8 N·m and 291rpm, since winding temperature reaches almost exactly the allowable temperature (113°C). Therefore, the application of LPTN to the control system of the motor drive will make it possible to predict the temperature under the corresponding torque-speed conditions, achieving the modulation of the required flow rate of the liquid coolant.

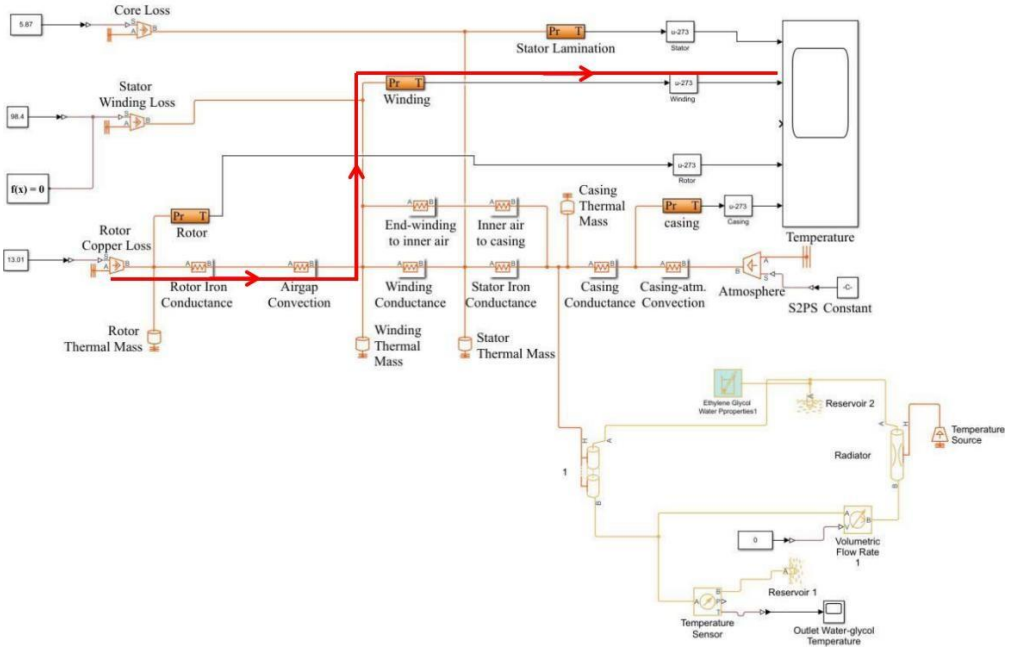

Fig.13 Modified LPTN model created in MATLAB simulink[18]

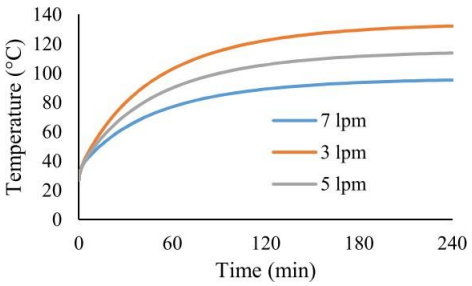

Fig.14 Winding temperature under the condition of 291 rpm and 4.8 N·m[18]

4. Cooling Methods in an EV motor

To put thermal management into effect on an EV motor, different cooling methods have been developed, which can be roughly divided into two categories: active cooling methods (such as fored air cooling, water cooling, oil cooling, etc.) and passive cooling methods (heat pipes, phase change materials, fins, potting materials, etc.). Additionally, it is emphasized that hybrid cooling methods have been proven to be more effective than a single one. This section will provide a detailed introduction and comparison of the aforementioned cooling methods.

4.1 Active Cooling Methods

In the cooling methods of EV motors, active cooling method refers to the technical means of actively regulating the motor temperature through external power sources or control mechanisms. Active approaches dissipate heat mainly by heat convection and heat conduction, so then controlling the motor temperature. Common methods of this kind comprise air cooling and liquid cooling. Most of the studies on active methods employ techniques like forced air convention and fluid flow cooling, among others. Thereby, the methods of air and liquid cooling are most frequently employed.

4.1.1 Air Cooling

Air cooling circulates air on the motor surface to dissipate heat, usually using devices such as fans to drive air to flow. When air flows over the surface of the motor, it will take away some heat generated by the motor. This method is relatively simple, lightweight, cost-effective, and has a simple structure that does not require additional coolant or complex circulation systems. However, its effect of heat dissipation is relatively poor. When the motor power is high or it operates under high load for a long time, simple air cooling cannot effectively remove enough heat in time, resulting in high motor

temperature. Hence, it is always used as a basic cooling method for motors that do not require particularly high heat dissipation. For a better cooling effect, other methods are needed in combination with air cooling.

Air cooling methods are mainly classified into two types—open-type and closed-type methods. The main difference between them lies in the air circulation mode and heat exchange mechanism. Open-type air cooling directly introduces external ambient air, which flows through the motor surface or internal heat dissipation channels, then discharges heat to the outside environment. Closed-type air cooling circulates air within a closed air duct, where heat exchange devices (such as radiators) regulate the air temperature for stable heat dissipation. The key comparison can be summarized in Table 2.

Table 2 Comparison of open-type and closed-type air cooling

Features	Open-type air cooling	Closed-type air cooling
Air source	Directly inhales external ambient air	Circulates air within a closed system
Temperature control capability	None	Can heat/cool air
Environmental impact	Thermal efficiency is affected by temperature, humidity and dust	High stability, adapts to complex environments
Cost and complexity	Low	High

In Ref. [19], Nakahama et al. study the cooling airflow within a one-way ventilated open-type EV motor. Fig.15 indicates the structure of this system. On the motor's side, a fan is installed in a separate position. The electric fan drives cold air into the motor via a rotating velocity component, which comes from the inlet of the bearing bracket. Generally, the airflow rate is larger, the cooling effect is higher. Nevertheless, if airflow diverges at the heat transfer wall, the air will become immobile, and the surface temperature of the heat transfer will rise. So, they design a novel structure to avert air separation and conduct a visualization experiment to verify the structure's effect.

In Ref. [20], Xu et al. propose a novel cooling structure for an open-type air-cooled induction motor shown in Fig.16. In this study, a rotor-mounted guide vane for axial ventilation is installed to enhance the cooling effect. As the motor operates, the guide vanes spin alongside the rotor, enhancing the trajectory and condition of the cooling gas flow within the terminal area and surrounding the rotor. The air circulation path is displayed in Fig.17. In the original motor, the peak temperature increase is situated in the stator windings, showing 121.44K. By contrast, the peak temperature decreases by 2.79K, accompanied by a 2.3% reduction in the proposed structure.

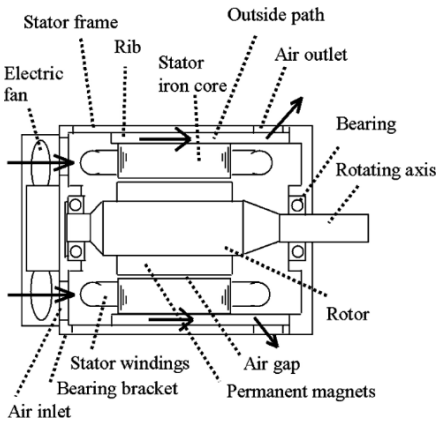

Fig.15 Structure of an open-type air-cooled EV motor [19]

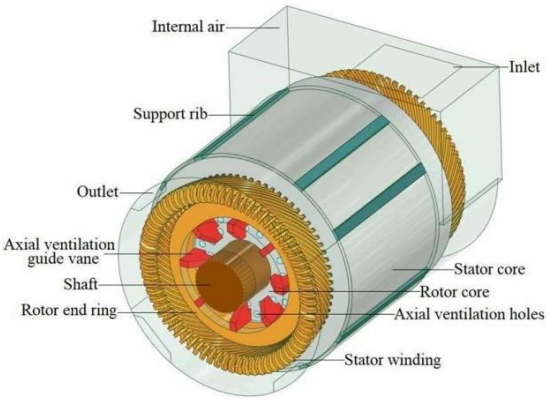

Fig.16 Enhancement structure of an open-type air-cooled induction motor [20]

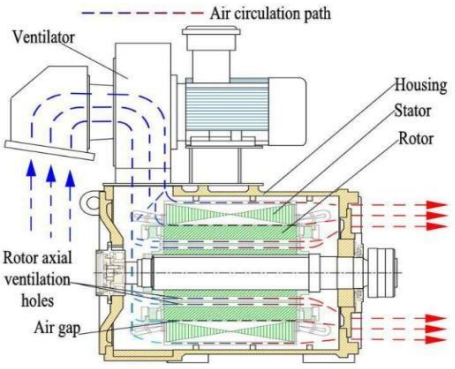

Fig.17 Diagram of the air flow trajectory of the motor [20]

As mentioned earlier, the cooling effect can be improved if air cooling is applied in a hybrid way. In Fig.17, the air entering the central region of the end space will collide with the air exiting axial ventilation holes of the motor, causing the vortex that obstructs smooth airflow, weakening heat dissipation effect. Therefore, in Ref. [21], Xu *et al.* study the cooling enhancement mechanism of the axial air deflector at the base of the study in Ref. [20]. As is shown in Fig.18, the air deflector is affixed to the interior side of the end cover on the air outlet side. Airflow will encounter the deflector, suppressing the vortex in the end space of the air outlet side, and then exit through the outlet, enhancing the cooling effect. Results from the simulation reveal fluctuations in both the peak and mean temperature increase of the stator winding with the axial size parameter (***La***) of the axial air deflector, concluding that the deflector achieve the best cooling ability with La=74.6mm. In this case, the maximum temperature rise is 113.8K which is 2.5K lower than before installation, while the average temperature rise of stator windings is 86.7 which is 1.9K lower than before installation. Furthermore, the simulation result accuracy is verified by an experiment.

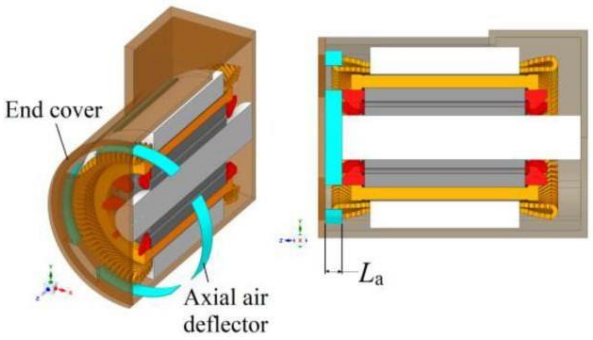

Fig.18 Schematic diagram of axial air deflector [21]

In Ref. [22], Mizuno *et al.* created a completely enclosed forced air-cooling mechanism for a traction electric motor. From Fig.19, the inner fan on the front side of the shaft forces air to circulate in the air gap and the rotor duct. Heat produced by the motor is conveyed to the ambient environment via the cooling unit (fins) on the casing. Then cooled air through cooling unit returns to the inner part of motor to continue cooling.

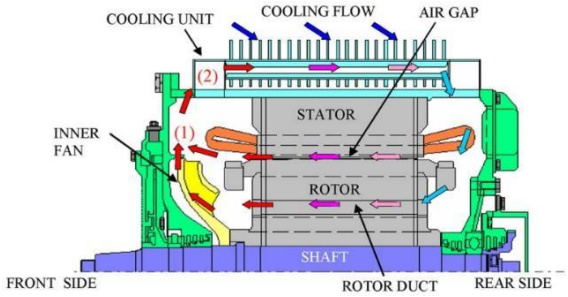

Fig.19 Sectional view of a totally enclosed motor [22]

In Ref. [23], Kim *et al.* use a 3D computational model of electromagnetic thermal coupling to investigate the cooling capability of air-gap fans for an IM. From Fig.20, the air-gap fan is secured on the rotary shaft at the end of the air gap between the stator and the rotor. Additionally, cooling air forced by an external fan enters into six inlets on the left side of the frame maintaining a steady flow rate, then traverses the air gap and ducts, exits through the six outlets on the right side of the frame at last. It should be noticed that ducts are formed by fins on the casing, indicating that this research is conducted by hybrid cooling methods instead of single air cooling to strengthen the cooling effect. By comparison of a motor without a fan, with one fan on one side, and with two fans on both sides, the results show the good effectiveness of the air-gap fan, which are summarized in Table 3 and Table 4.

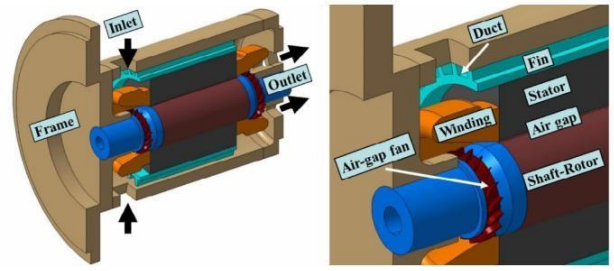

(a)Isometric view (b) Enlarged isometric view

Fig.20 Diagram of an induction motor featuring air-gap fans [23]

Table 3 Comparison of temperature conditions of different parts in an IM

Case	Rotor Max Temp. /℃	Winding Max Temp. /℃	Avg. Temp. /℃			
			Rotor	Winding	Stator	Frame
Without an air-gap fan	324	143	302	139	114	44
With an air-gap fan	245	121	216	115	96	41

Table 4 Comparison of HTC increase by air-gap fan

Case	Winding HTC Increase Compared to the Case without Air-gap Fan (%)	Air Gap HTC Increase Compared to the Case without Air-gap Fan (%)
With both air-gap fans	29 ~ 31	64 ~ 90
With a single air-gap fan (front)	15 ~ 17	28 ~ 43
With a single air-gap fan (rear)	7 ~ 8	51 ~ 71

Air cooling systems are mainly employed alone in low-power EV motors, or in combination with liquid cooling systems in high-power EV motors. Obviously, air cooling is indeed effective in some degree. However, since it's relatively low heat transfer coefficient, the electric motors of EV are mostly cooled by a liquid cooling system nowadays that consists of

water cooling and oil cooling [24]. Regularly, water circulates through the jacket's cooling channels, while oil moves inside the motor to reduce the heat of the hot spot. Liquid cooling will be described in detail in the next parts.

4.1.2 Liquid Cooling

Inside the motor, liquid cooling flows via coolant, directly soaking up the motor's heat and subsequently releasing it through a radiator. The advantages of liquid cooling over air cooling can be summed up into the following aspects.

Efficient heat dissipation mechanism

Heat conduction efficiency of liquid cooling is increased by 3 to 5 times, heat dissipation speed is faster, and temperature uniformity is better than that of air cooling.

Extension of EV motor lifespan

The liquid cooling system reduces damage to internal components caused by thermal expansion and contraction through precise temperature control, thereby extending the lifespan of the motor.

Liquid cooling is categorized based on coolant type into three types: water cooling, water and ethylene glycol mixture and oil (lubricant) cooling, which are coolants with high specific heat capacity.

Water acts as a kind of coolant characterized by its elevated thermal conductivity and significant specific heat capacity. Moreover, water is pollution-free and low-cost. These characteristics make water widely used. To address the issues of water's high freezing and low boiling points, a mixed solution of water ethylene glycol is employed to lower the medium's freezing point and enhance the water-cooled cooling system's adaptability to the environment. In addition, water cooling is prone to corrosion of the casing during long-term operation, so additives such as anti-corrosion should also be added during use.

Based on the cooling mode, another classification method is to divide liquid cooling into water cooling and oil cooling. Furthermore, based on whether or not it cools internal parts such as windings, oil cooling methods can be divided into direct oil cooling with oil-immersion type and oil-spray type, and indirect oil cooling. Oil-immersion type utilizes the insulation properties of oil to directly introduce oil into the interior of the electric motor, immersing the stator and roto r, which can effectively enhance HTC inside the motor. However, oil-immersion type will cause friction between the rotor and oil during operation, reducing the motor’s efficiency. Oil-spray type sprays oil onto the end of stator windings and other components for cooling. Indirect oil cooling is the process of circulating oil through the hollow motor shaft and motor housing for heat dissipation, which can directly remove the motor’s internal heat with less friction loss with the rotor.

In Ref. [25], Satrústegui *et al.* study the water cooling for an IM. Their analysis encompasses the water jacket's design, key parameters, and certain correlations relevant to the design of cooling ducts. They also show four topologies of water jackets shown on Fig.21. The distinction between them is evident in the decrease in pressure they introduce to the cooling circuit during the analysis of various topologies with the identical cooling surface. Specifically, the pressure drop will rise with the increasing number of bends or splits introduced into water jackets. The subsequent pair of parameters will constitute the foundation of the design process: the fixed water flow rate (m^3/s), $\boldsymbol{Q_{water}}$; the maximum pressure drop (Pa), $\triangle \boldsymbol{P_{max}}$ [25]. According to the comparison in Table 5, spiral water jackets are identified as the optimal option for minimizing the pressure drop.

Table 5 Pressure drop of topologies of different water jackets [25]

Geometry	Cooling surface (mm^2)	Pressure drops (Pa)
Spiral	118,760	16309.7
U-shaped (one duct)	119,010	46896.5
U-shaped (bifurcated)	110,278	106092.8
Axial	117,768	155656.9

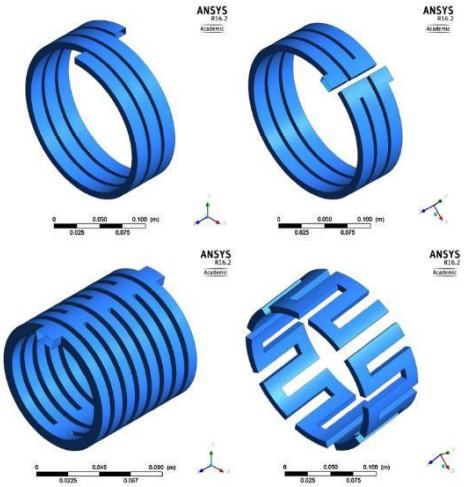

Fig.21 (a) spiral, (b) U-shaped (one duct), (c) U-shaped (bifurcated), *and (d) axial water jacket.*[25]

Fig.22 shows five parameters defining the water jacket with rectangular ducts: distance between the cooling ducts and the stator stack ($h_{Fe,water,ch}$); distance between the cooling ducts ($w_{water,ch,space}$) ; axial length ($l_{water,\ jacket}$); width of the cooling duct ($w_{water,ch}$); height of the cooling duct ($h_{water,ch}$). By an thermal model and CFD simulations, it is concluded that $h_{Fe,water,ch}$ should be defined as low as possible because of its escalation leading to the temperature increase of the stator with the material of stainless steel or steel carbon 1%; the impact of $w_{water,ch,space}$ on machine temperature is not high; $l_{water,jacket}$ has a direct correlation with the water jacket's overall length (L_T) which has direct influence on two vital design parameters: the cooling surface ($A_{cooling}$); the pressure drop ($\triangle P$). So L_T should be designed to achieve maximum $A_{cooling}$ with the consideration of its limit by $\triangle P$; the area of the rectangular cooling duct is related to the peak water flow rate (Q_{water}) and the peak water speed ($v_{erosion}$) , and the design criterion of cooling ducts should meet the function below; the contact between the stator and the housing is significant to optimize the water jacket, and good contact results in good thermal performance; the temperature decreases as the diameter of the shaft (D_{shaft}) widens, so choosing the appropriate diameter for the shaft plays a crucial role in optimizing rotor temperatures.

$$w_{water,ch} \cdot h_{water,ch} > \frac{Q_{water}}{v_{erosion}}$$

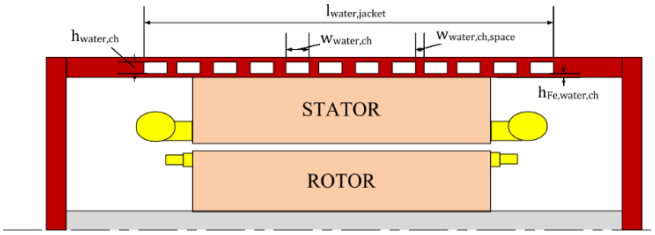

Fig.22 Parameters defining the water jacket [25]

In Ref. [17], Li *et al.* studied an oil-water composite cooling system which is a new kind of direct cooling. The configuration of the system is displayed in Fig.23. The ability to transfer heat was improved by implementing a forced liquid cooling method via spiral cooling ducts. The cooling oil completely immerses the stator, directly cooling the stator [17]. The innovation point in the research is that the oil used to cool the motor is not cooled by additional cooling devices but pumped into the housing and cooled by cooling water flowing in the water tube inside the housing through heat convection. At the same time, the original water jacket of the casing is used to maintain the function of the cooling motor [17]. In fact, this cooling method is a hybrid composed of oil and water cooling.

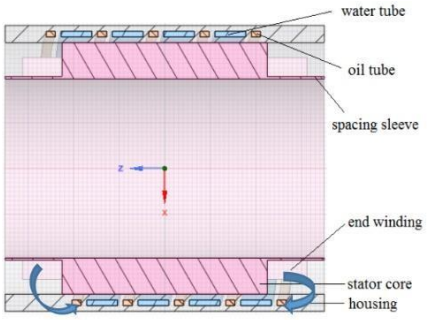

Fig.23 Configuration of an oil-water composite cooling system [17]

The research proposes three types of cooling structures from Fig.24 to Fig.26, in which the focus of the design is on the oil and water channels inside the housing. The objective is to fully realize heat exchange between oil and water, reduce the temperature of oil at the outlet, and enable water to cool the stator at the same time. In No.1, the oil and water channels are designed in a "C" shape; In No.2, the oil flow channel and water flow channel are distributed up and down, and the oil can directly contact the stator, relying on the coordination between the motor and the casing to form an oil flow channel; In No. 3, the oil flow channel and water flow channel are designed with a double helix[17].

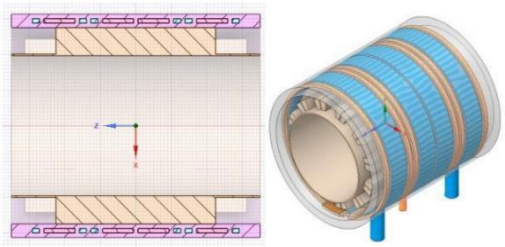

Fig.24 Structural of cooling design for No.1[17]

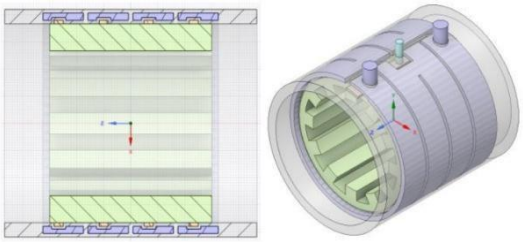

Fig.25 Structural of cooling design for No.2[17]

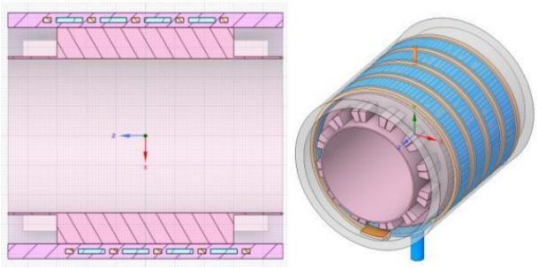

Fig.26 Structural of cooling design for No.3[17]

By numerical simulation, the results are shown in Table 6. According to the comparison, temperatures of outlet oil of No.1 and No.3 are more or less the same, which are higher than that of No.2. Average temperatures of the inner wall of the casing of No.1 and No.3 are also close, which are lower than that of No.2. Although the form of channel structures of No.1 and No.3 are different, the difference is not that significant. After all, cooling oil in these two designs does not directly contact the stator. However, the heat transfer path changes in No.2. At the base of the difference above, there are differences in application of the three designs. No.1 and No.3 are more suitable for motors with high stator core losses, while No. 2 is more suitable for motors with high winding losses [17].

Design	Temperature of outlet oil (K)	Average temperature of the inner wall of the casing (K)
NO.1	319.27	317.05
NO.2	310.89	320.56
NO.3	319.07	318.06

Table 6 Results [17]

In Ref. [26], Zhang *et al.* proposes an innovative model of liquid-cooled PMSM energy system for an EV and does research at the basis of this model via numerical simulation to verify the escalation in the output power of the energy system. As for the aspect of liquid cooling effect, they compare and analyze the temperature and pressure drop under different inlet flow rate of coolant for an EV PMSM using the same and the most commonly employed housing water jacket. Simulations are conducted under the rated condition of 3500r/min and from the current of 140A. Simulation results can be seen in Fig.27 and Fig.28. According to temperature calculation results, it is shown that the PM temperature is 11.64℃ more but the pressure drop reaches 93kPa less at 3L/min than at 30L/min. It is apparent that the flow rate of coolant has great influence on the liquid cooling effect.

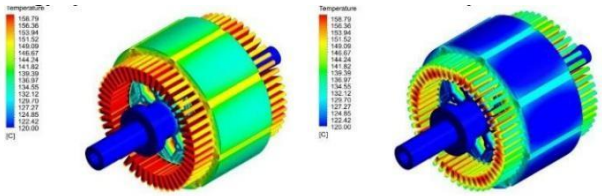

V_1=3L/min (3500r/min; 140A) V_1=30L/min (3500r/min; 140A)

Fig.27 Temperature field of PMSM under different inlet flow rate [26]

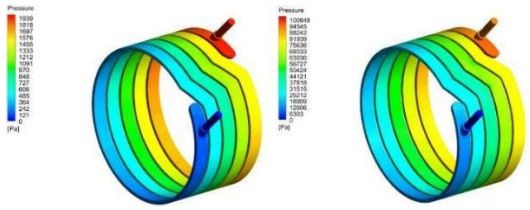

V_1=3L/min (3500r/min; 140A) V_1=30L/min (3500r/min; 140A)

Fig.28 Pressure of PMSM cooling circuits under different inlet flow rate [26]

As for real traction motors, diverse flow paths are engineered inside the water jacket to optimize the cooling efficiency. In Ref. [27], however, Park et al. conduct a case where there is no specific flow path inside the water jacket. Apart from water jacket cooling (WJC), they also propose other three cooling techniques, such as direct slot cooling (DSC), end-tip cooling (ETC) and channel cooling (CHC). The structures of them are displayed in Fig.29. In WJC, the stator is cooled by coolant flowing through its water jacket and various paths are designed in WJC to optimize the cooling performance; In ETC, caps are at both ends of the motor as in DSC. Nevertheless, as the cooling oil fed into the header cap does not pass through the slot and exits via the outlet nozzle on the reverse side of the same header cap, it directly reduces temperatures of only certain sections of the winding; In CHC, cooling channels are fixed in the slots to directly contact windings; In DSC, the cooling oil entering a top header cap is allocated across 12 slots for direct coil cooling and released from the opposite header cap. By simulation and experimental verification, DSC achieves the best performance among the four types in general.

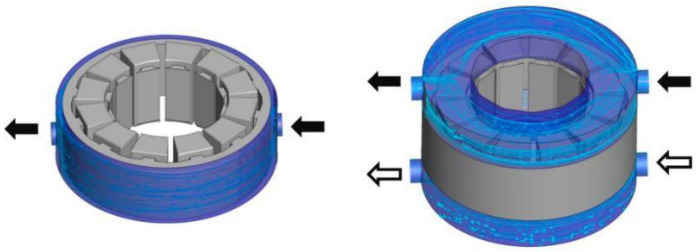

(a) Water jacket cooling (WJC) **(b) End tip cooling (ETC)**

Fig.29 Four different types of coolant path lines [27]

In Ref. [28], Li Ye *et al.* also proves the favorable cooling effect for the hybrid way in an experiment, in which both water and oil are used to cool the motor. However, the uniqueness lies in the fact that the oil cooling utilizes spray cooling, another kind of direct cooling. The oil cooling structure can be seen on Fig.30. In this method, cooling water through the water jacket indirectly cools the motor, while cooling oil is ejected through the nozzles fixed on the end cover to spray onto end windings for direct cooling. The research is conducted via an experiment test. The experiment conditions are shown in Table 7. (n—the motor speed; T_m—the motor torque; Q_w—the flow rate of cooling water; $\triangle P$—the pressure difference between inlet and outlet of the water jacket; Q_o—the flow rate of cooling oil; P_{in}—the inlet pressure of oil) Composite cooling's impact on temperature reduction is obvious, and the conclusion can be summed up below through the experiment:

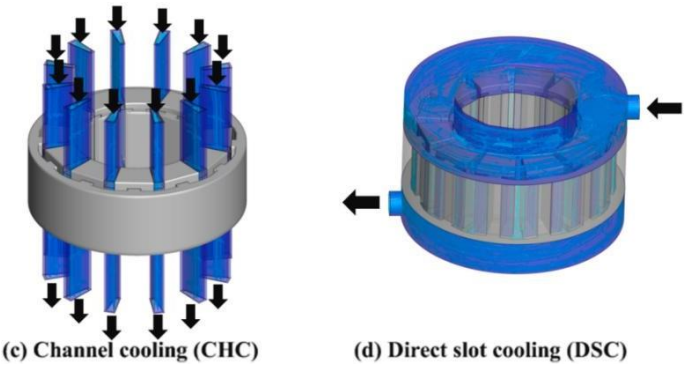

(c) Channel cooling (CHC) (d) Direct slot cooling (DSC)

Under the no-load condition of 3200rpm, the temperature rise decreased by 52.5% when No.2 working condition (both oil and water cooling) than No.1 (only water cooling) [28].

Under the load condition, the temperature rise decreased by 40.2% when No.4 working condition (both oil and water cooling) than No.3 (only water cooling) [28].

Oil spray cooling consistently outperforms oil immersion cooling in terms of cooling efficacy. The oil spray cooling for electrical machine seems a promising solution. But it still needs more development and research work [29].

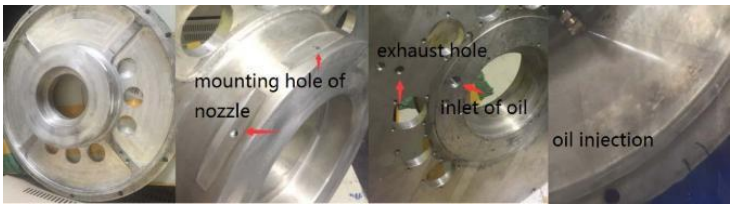

Fig.30 Motor end cover [28]

Table 7 Experiment Condition [28]

NO.	n/rpm	T_m/N·m	Q_w/(m^3 /h)	△P/KPa	Q_o/(m^3 /h)	P_{in}/MPa
1	3200	11	3.0357	37.9	0	0
2	3200	10	3.0972	39.2	0.5688	0.084
3	1900	400	3.0972	39.2	0	0
4	1900	400	3.1170	39.8	0.5450	0.104

Cooling methods above generally focus on the modification of the stationary parts such as the stator or housing of an electric motor. Actually, the rotor can be also reformed for cooling. In Ref. [30], Deriszadeh *et al.* initially proposed a baseline model marked by the movement of cooling fluid within the hollow shaft which is displayed in Fig.31(a). Cooling fluid enters the inlet of the hollow shaft on one side and exits the outlet on the other side. The rotation of the shaft improves the efficiency of the heat transfer, resulting in additional turbulence to the flow. Admittedly, this structure can evacuate the heat of the rotor to some extent. Nevertheless, its cooling effect is limited especially under the situation of high-power operation of the motor due to the only one fluid path. To improve this situation, a modified configuration of shaft is

proposed shown in Fig.31(b). Especially, a stationary inner tube fixed on the motor housing is situated inside the outer shaft, which rotates at the identical rotor's angular speed. Cooling fluid enters the inlet of the inner tube (open end) and flows to the other side (closed end). Then cooling fluid returns to the open end through the annulus gap between the inner tube and outer hollow shaft. Due to the spirals attached to the external surface of the inner tube, the path of cooling fluid traces along helical trajectories during the rotation of the outer shaft. This causes the enhancement of turbulence, giving rise to the increase of the convective HTC between the outer hollow shaft and the cooling fluid to reduce the rotor temperature. By simulation analysis, the temperature of the external cylindrical surface of the shaft (i.e. the temperature of the internal surface of the rotor) decreases from 110℃ to 80℃ in the proposed model, 30℃ lower than the baseline model with direct single-flow cooling system of the rotor shaft, verifying the effectiveness of this structure.

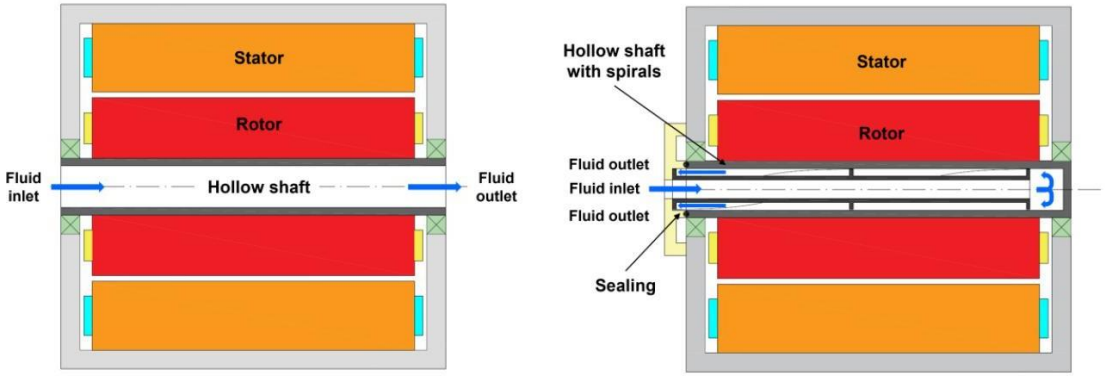

(a)Baseline model (b) Proposed model

Fig.31 Rotor shaft cooling methods [30]

In Ref. [31], Liu *et al.* compare the cooling capability of three cooling models. As is displayed in Fig.32, arrows indicate the flowing direction of the coolant. Model A is the axial housing liquid cooling model; Model B is the oil spray cooling and axial housing liquid cooling model; Model C is the hollow shaft cooling and axial housing liquid cooling model. Actually, Model A is a traditional water jacket cooling, where coolant flows axially through the oil channels within the housing. Model B features ring-shaped oil grooves positioned at the front and rear end windings, with 16 evenly spaced oil spray holes on the grooves. Oil emitted from the spray holes lands on the shaft, and due to centrifugal force, a portion of the coolant is thrown onto end windings, amplifying the cooling impact on end windings. The configuration of Model C is the same as that of Model A, except for the shaft. Model C has a hollow shaft, into which coolant flows from the inlet on the one side to the outlet on the other side. During the temperature rise calculation, parameters are set as below:

the inlet flow rate of the coolant: 10L/min.

the inlet temperature of the coolant: 65℃.

the ambient temperature: 40℃.

the rated speed of the motor: 6000r/min.

the internal coolant volume flow rate of the shaft in Model C: 2L/min.

The results are shown in Fig.33. Model B achieves the best cooling capability, of which the steady-state temperature rises for the windings, stator core and PMs are 126.44℃, 119.79℃ and 79.69℃, respectively. This is because Model B has both oil spray cooling and water jacket cooling, the latter of which can directly contact the interior of the motor, quickly dissipating the heat.

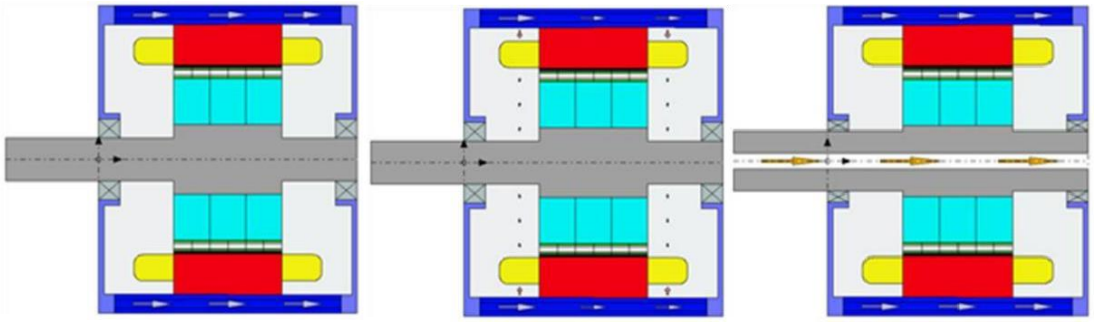

a)Model A b) Model B c) Model C

Fig.32 Comparison of structures of three cooling models [31]

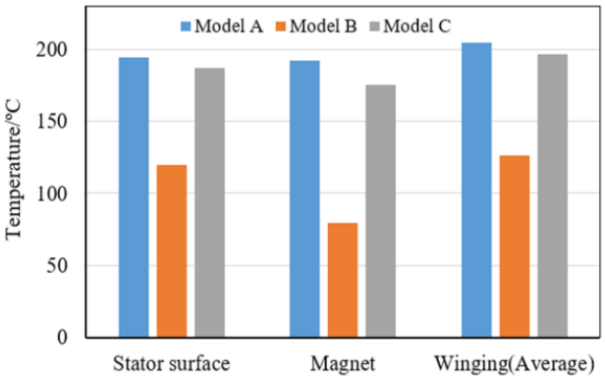

Fig.33 Comparison of steady-state temperatures of typical motor components in three models [31]

4.2 Passive Cooling Methods

A passive technique does not need additional devices while active method requires the use of external devices such as pumps, nozzles etc. [32] For an electric motor application, the passive method is preferable to reduce complexity [32]. This type of technique has the merits of simple structure, high reliability, and low energy consumption, but it also has the problem of limited heat dissipation capacity. Commonly used passive techniques comprise fins, heat pipes (HPs), phase change materials (PCMs), and potting materials.

4.2.1 Fins

The losses cause a temperature rise which may result in large thermal load on components of the motor. In order to prevent that, finned motor housing is applied as its extended area of the outer surface enhances heat dissipation to the environment, thus facilitating temperature stabilization and keeping of the acceptable operating conditions [33]. The geometry of fined housing is displayed in Fig.34.

In Ref. [34], Sibi *et al.* study the fins with three geometry designs for a BLDC shown in Table 8. The thickness of each fin is 2mm, and the depth of each fin can be seen in the first column in Table 8. By simulation analysis, the table shows that with the increase of the fin depth, the temperature of windings decreases, and the heat transfer rate of windings increases. Moreover, the results also show that the fins on the housing can reduce the temperature of end windings up to 17%.

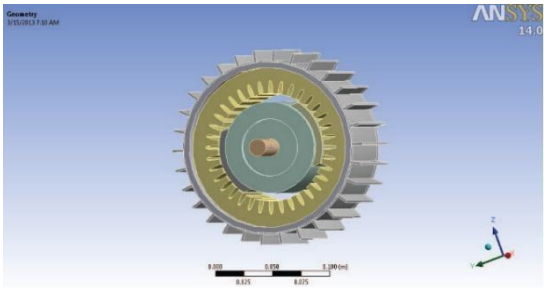

Fig.34 Fin geometry at the motor housing[34]

Table 8 For fines: temperature & rate of heat transfer [34]

S.No	Temperature and Heat transfer rate		
	Fins (mm)	Temperature (℃)	Rate of heat transfer (W)
1	5mm (or) 0.005m	59.42	141.48
2	10mm (or) 0.01m	55.48	204.33
3	20mm (or) 0.02m	49.13	244.68

In Ref. [35], Pronin *et al.* study the impact of the orientation of causing fins on the operating temperature of the PMSM's active parts. Fig.35 displays four designs taken into discussion such as (a) cross fin design (outlets), (b) longitudinal fin design (outlets), (c) cross fin design (side), and (d) longitudinal fin design (side). The simulation results show that longitudinal cooling fins on the outlets and transverse fins on the side achieve the best cooling effect compared with the baseline model without fins. Specific information is shown in Table 9.

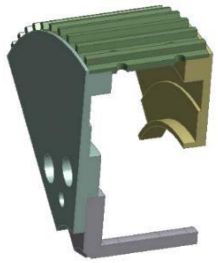

(a) Case with transverse fins (outlets)

(b) Case with longitudinal fins (outlets)

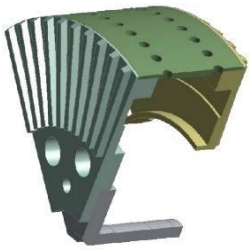

(c) Case with transverse fins (side)

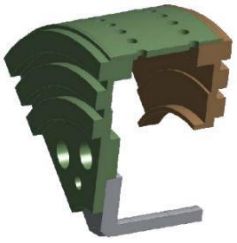

(d) Case with transverse fins (side)

Fig.35 Different orientations of casing fins [35]

Table 9 Results of thermal calculations [35]

	Max. winding temperature, ℃	Max. PM temperature, ℃
Without fins	182.7	179.7
Cross fins (outlets)	201.1	162.6
Longitudinal fins (outlets)	172.2	157.7
Cross fin design (side)	163.8	135.6
Longitudinal fin design (side)	176.6	162.4

4.3 Heat Pipes

The heat pipe (HP), a passive thermally conductive medium, characterized by its high conductivity, enables swift heat transfer across vast distances with minimal temperature reduction, straightforward design, and the absence of external pumping energy. Heat pipes, known for its superior heat transfer capabilities, boasts notable thermal conductivity, superior

isothermal characteristics, variability of heat flow density, and environmental adaptability, making it an exceptionally efficient and lightweight cooling technique. With its excellent heat transfer performance, heat pipes not only improve the effectiveness of traditional cooling methods but also increase entirely new heat transfer pathways [36]. A standard HP is made up of a sealed tube, a wick configuration, and channels for vapor. Its physical diagram and working principle are displayed in Fig.36 and Fig.37 respectively. The operation process of a heat pipe primarily comprises four stages:

Stage 1: evaporation.

Stage 2: heat transfer.

Stage 3: condensation.

Stage 4: return.

Specifically, the hot part of the HP (evacuation section) is placed at the hot spot of a motor, such as the end of windings or the stator, and the cold part (condensing section) is placed outside the motor. The heat generated by the motor is transferred to the evaporation section and absorbed by the liquid working medium. The medium in this part vaporizes and the steam moves to the condensing section through the adiabatic section for heat release and liquefaction. The motor's heat dissipation system is established through the repetition of a heat exchange cycle in which the liquid working medium reverts to the evaporation section under capillary pressure.

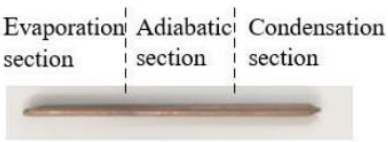

Fig.36 Physical diagram of the HP [37]

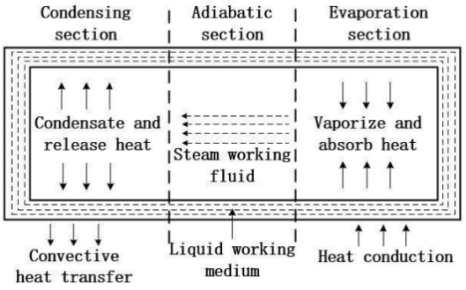

Fig.37 Working principle of the HP [37]

In Ref. [38], Geng *et al.*designedn a HP-based cooling system for PMSM and discussed the geometric structure of the HP. From Fig.38, L-shaped HPs are embedded into the end cover of the motor with the evaporation section placed near the end of windings. And the condensing section of HPs are placed outside the motor. From Fig.39, optimization of the dimension and the geometric shape of an HP with the change of HP angle α is conducted to enhance its cooling efficiency for the motor. By FEA simulation, the results illustrate that the peak temperature at the winding ends is up to 100.45℃ with the corresponding temperature increase of 75.45℃ in conventional water-cooled motor without HPs, While the peak temperature at the winding ends is 93.47℃ with a temperature rise of 68.47℃ in the motor with HPs. Furthermore, the cooling performance of HPs varies with the change of HP angle α, achieving the best at HP angle of 30° .

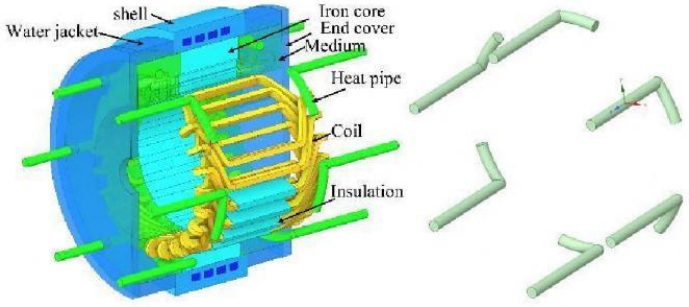

Fig.38 Design of motor with water cooling based on HPs [38]

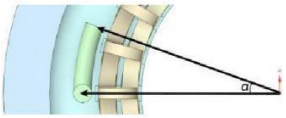

Fig.39 HP angle α [38]

In Ref. [36], Chai *et al.* compare the effects of HPs in different positions in the slot on the temperature rise of the motor, which can be seen in Fig.40. From the left to the right, HPs are positioned in the notch, in the central section of the slot and in the bottom of the slot respectively. By simulation, the results show that the HP positioned in the central section of the slot achieves the best cooling effect, of which the maximum winding temperature is 5℃ smaller than that of the other two types.

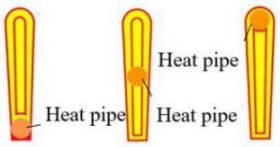

Fig.40 Different HP positions in the slot [36]

In Ref. [39], Gu et al. make further improvement to HPs for an axial flux PMSM with air cooling. From Fig.41, the evaporation section of the HP is inserted into the stator slot to provide an auxiliary cooling path for the winding, and the stator core and heat pipes are arranged at the centerline of the slot winding for maximization of the uniformity of heat dissipation; The condensation end of the heat pipe is connected to an aluminum radiator. Fig.42 shows the structure of the aluminum radiator. It is used to enlarge the cooling area and remove heat from the condensation section of HPs due to the contact area between HPs and external environment is small, causing the limited cooling effect. The investigation of dimensions of the radiator is conducted, showing that the maximum temperature of windings, the stator core and PMs of the motor decreases with the radial length H and fin length R of the radiator increasing. When H is greater than 90mm or R exceeds 18mm, the heat dissipation capacity tends to be saturated. So, H and R are determined to be 90mm and 18mm respectively.

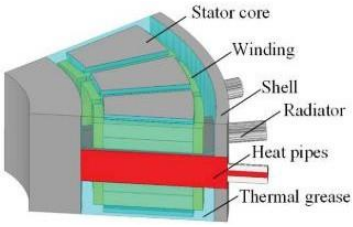

Fig.41 Motor cooling system structure diagram [39]

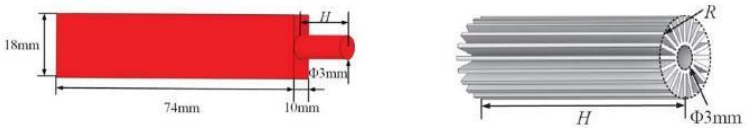

(a) HP (b) Radiator

Fig.42 Diagram of the cooling structure [39]

4.3.1 Phase Change Materials

Traditional passive cooling techniques employ fins affixed to the motor housing's outer surface, designed to enlarge the housing's surface area, thereby enhancing the efficiency of heat transfer. However, the disadvantage of fins lies in the fact that its cooling efficiency is minimal, making it better suited for the well-ventilated situation. PCMs are a great supplement to fins. In passive cooling applications, PCMs, serving as phase-change thermal storage materials, have garnered significant interest due to their benefits like high latent heat of fusion, high specific heat, adjustable temperature stability, and minimal volume alteration during phase change. Possessing such outstanding thermal characteristics, the PCM-based strategies have exhibited excellent performance for thermal management area [40].

In Ref. [41], Wang *et al.* present the design of an PMSM with PCM cooling. Paraffin is used as PCM filled in the hollow motor casing, of which the model is shown in Fig.43. They compare the temperatures of the casing with paraffin and that without paraffin on continuous operating condition and on duty cycle 600s:1800s respectively. The results are displayed

in Fig.44. (T_c—the transient temperature of casing without paraffin; T_a—the maximum transient temperature of the aluminum part; T_p—the minimum transient temperature of the paraffin part of the casing with paraffin) On the continuous state with the initial temperature of 298.15K, T_a exceeds 373.832K for 650s while T_c exceeds 373.167K for 438s. On the duty cycle state, the highest and lowest temperatures of the paraffin-free casing are respectively 410.551K and 334.000K while those with paraffin are 409.187K and 354.056K in the stable temperature period. Obviously, the impact of paraffin in regulating the casing's temperature is significant.

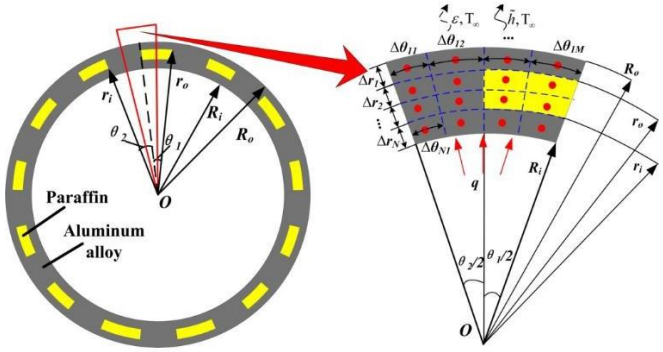

Fig.43 Simplified casing model with paraffin and nodes setting for temperature calculating [41]

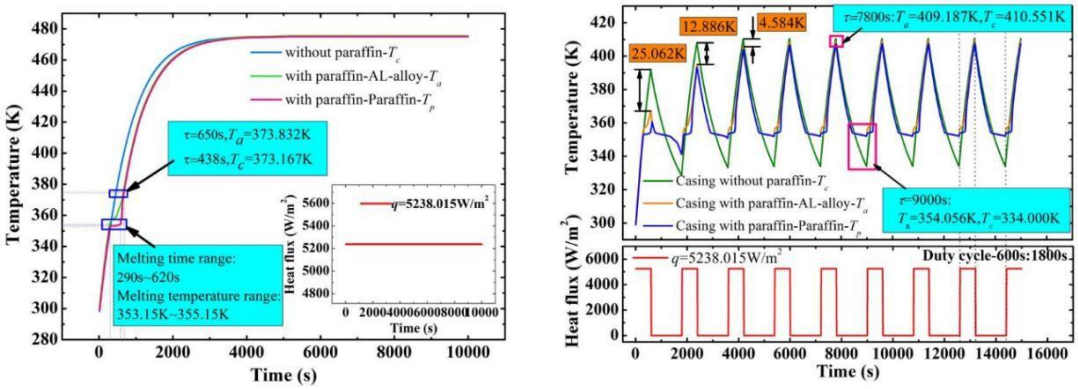

(a)on continuous operating condition (b) on duty cycle 600s:1800s

Fig.44 Transient temperatures of different models of motor casings [41]

In Ref. [42], Zhang *et al.* study PCM cooling performance of suppressing the transient temperature increase of the motor casing filled with 64# paraffin, a kind of PCM with high latent heat, minimal volume change, non-corrosiveness, and ease of encapsulation. They use enthalpy-porosity method to simulate the latent heat behavior of PCM melting. Furthermore, they conduct comparisons for five cases with different PCM filing amounts which are displayed in Fig.45. The simulation results verify the positive role of PCM to temperature rise suppression during the melting process and show that the larger amount of PCM filling does not necessarily lead to a better effect. Case 1 with the PCM filling thickness of 2mm, the smallest amount, proves the best motor overload extension capability with the time extended by 6.5 seconds, and the maximum temperature rise suppression capability with 10.6K.

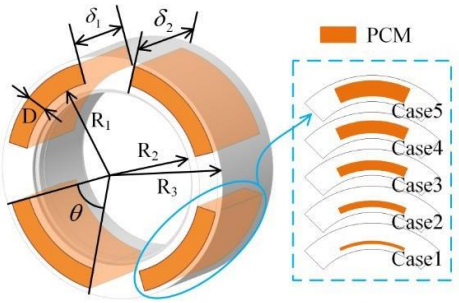

Fig.45 Five cases with different PCM filling amounts [42]

4.3.2 Potting Materials

Potting materials, as a key thermal management solution, achieve the following functions by filling the gaps in the motor stator winding, ends, and slots: efficient heat conduction & reliable electrical insulation. Use of potting materials results in the remarkable decrease of winding temperatures and the increase of motor power density. Potting the stator windings provides a direct thermal connection to the motor housing, which has been shown to reduce winding temperatures by up to 50℃ at a given power output, and increase power output by 15-25% at a given temperature, compared to an unpotted motor [43][44][45]. The favored potting materials are silicone, epoxies and urethanes.

In Ref. [46], Nategh *et al.* study two main potting methods—the end winding potting & the global winding potting. Both of the two methods are conducted through experiments. The process of the two methods is conducted in the study, and the final products are displayed in Fig.46 and Fig.47 respectively. In the case of end winding potting, the comparison of the unpotted motor, the potted motor with potting material with the thermal conductivity of 1.1W/m·K and 3.5W/m·K is implemented. The simulation results show that with the same active motor length, potting materials have good effects on the reduction of winding temperatures. Furthermore, the higher thermal conductivity of the potting material leads to improved cooling efficiency. In the case of global winding potting, the comparison of the unpotted motor with conventional impregnation material with the thermal conductivity of 0.2W/m·K and 1.1W/m·K, and the potted motor with potting material with the thermal conductivity of 1.1W/m·K is implemented. The results also verify the effect of heat dissipation of potting materials. In addition, experiments are conducted for the confirmation of the effect of potting materials and comparison of different cases. The experiment results illustrate a substantial decrease in temperature in both steady state and transient state in the case of global and end winding potting compared with the case of non-potted motor.

Fig.46 Final product in the case of end winding potting [46]

Fig.47 Final product in the case of global potting [46]

4.4 Hybrid Cooling Methods

Hybrid cooling methods are an innovative solution combining the advantages of multiple cooling methods, including active-active, active-passive, or passive-passive, aiming to improve heat dissipation efficiency, adapt to complex working conditions, and ensure the motor performance and lifespan. Due to the distinctive cooling capability, hybrid cooling methods are adopted in most cases instead of unique cooling methods.

In Ref. [47], Lee *et al.* use a hybrid cooling method by combining housing jacket cooling and hollow shaft cooling, i.e., the active-active hybrid cooling method. The schematic diagram is displayed on Fig.48. They compare the present method (hollow shaft oil cooling + housing cooling) with other methods (general oil cooling for stator, oil spray cooling for coil

and housing) via experiments. The results indicate that the highest rotor temperature is 77℃, 147℃ and 107℃ respectively, and that of the stator is 60℃, 104℃ and 89.8℃ respectively, verifying the effect of the hybrid cooling.

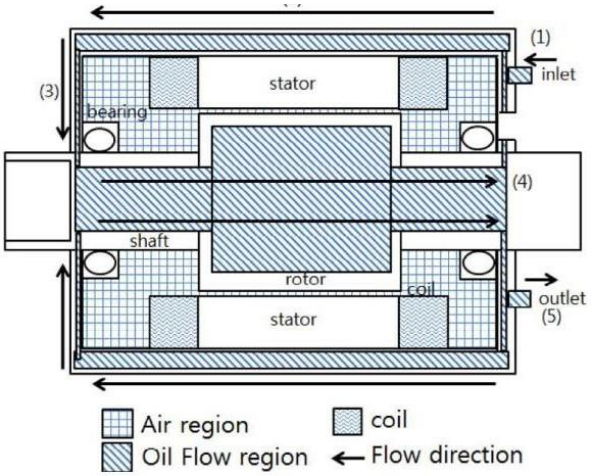

Fig.48 Proposed cooling method: 2D coolant path [47]

In Ref. [48], Huang *et al.* study the cooling effect of a hybrid cooling system with the combination of liquid cooling, HPs, fins and forced air cooling, i.e., the active-passive hybrid cooling method. Fig.49 displays the configuration diagram of the hybrid cooling system. A hybrid cooling solution is provided by the cradle design by incorporating a helical coolant jacket for the liquid and a series of slots for the HPs. One end of an HP is embedded in the axial slot; To increase the heat transfer area, the other end of an HP is equipped with an array of circular fins. A centrifugal fan is installed inside the HP structure to provide forced heat convection. The simulation results confirm its outstanding cooling and energy-saving capability, showing that the motor temperature is maintained near the desired value of 70℃ and up to roughly 370 kJ of energy is conserved compared with a conventional liquid cooling system for an electric motor with 85 kW within 1500s run time.

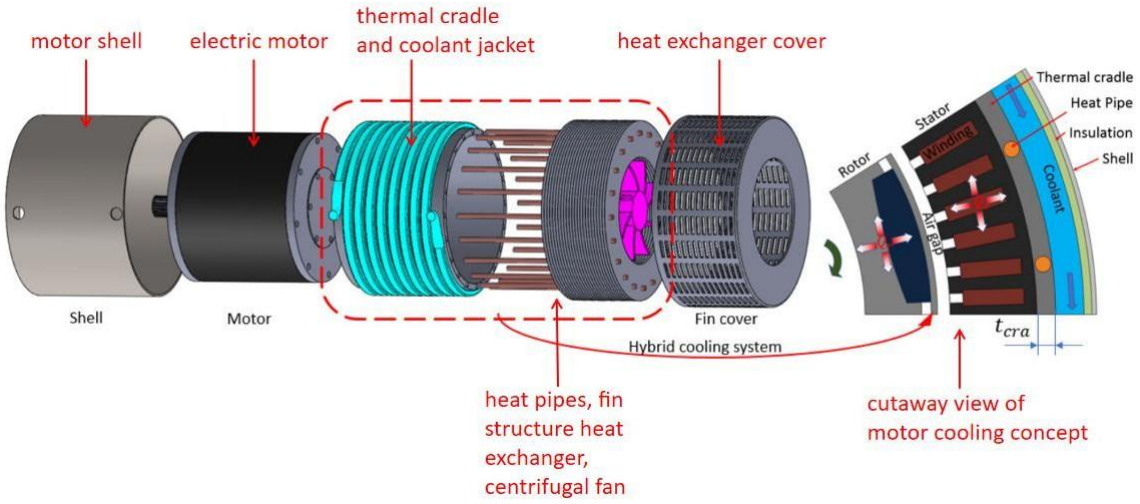

Fig.49 Configuration of the cooling system for electric motors [48]

In Ref. [49], Yuan *et al.* compare three motor prototypes, including the original prototype (M-P), the prototype of three-dimensional rounding module (M-RM) and the prototype of straightly embedded module in enclosure (M-SEME). The latter two adopt passive-passive cooling methods, of which the diagrams are shown in Fig.50. By numerical simulations and experimental tests for the comparison of effectiveness of different prototypes under different rated conditions, the results show that M-SEME achieves the best cooling effect among all the three prototypes under all rated conditions. It is displayed on Fig.51.

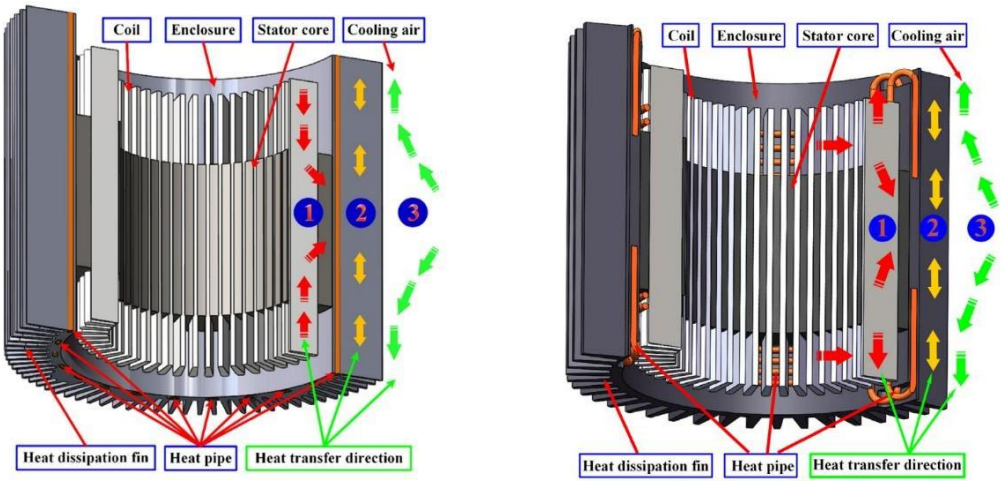

(a)SEME (b) RM

Fig.50 Cooling principles of an air-cooled PMSM with HPs [49]

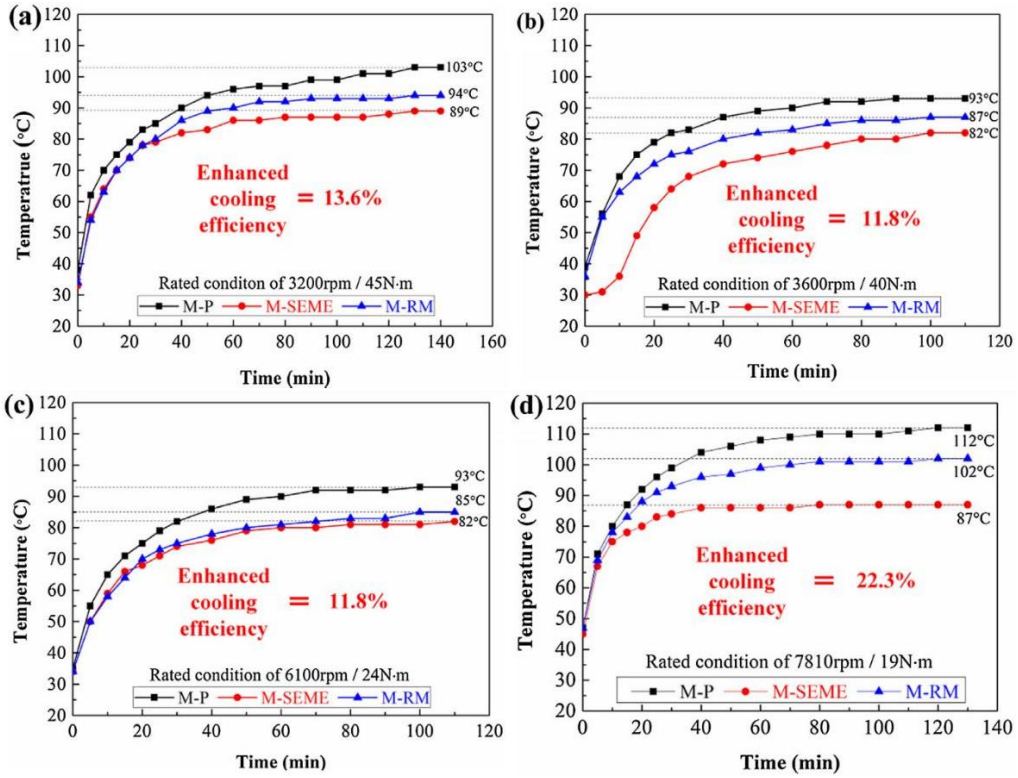

Fig.51 Curves depicting the increase of temperatures over time in various rated conditions [49]

5. Summary

Sections above introduce different kinds of cooling schemes in detail. In this section, the key information of cooling schemes described in some relevant references will be summarized in the appendix at the end of the text.

6. Conclusions

This review article briefly describes the structure, the working principle and characteristics of an EV motor (PMSM), subsequently leading to its heating mechanisms, which do harm to the motor and need to be constrained. Then analysis

and calculations of motor losses are introduced in detail. The most important part of the article is the description of common cooling methods which are pivotal to ensure efficient and safe operation of an EV motor. At the basis of the entire text, the following key points can be concluded:

Common calculation methods of motor losses consist of numerical methods (FEA & CFD) and LPTN. FEA and CFD are based on complex numerical methods and are suitable for high-precision analysis; LPTN provides solutions quickly by simplifying the model. The three methods need to be selected according to specific situations.

Cooling methods are mainly classified into three parts - active cooling methods, passive cooling methods and hybrid cooling methods. Active cooling methods include forced air cooling, water cooling and oil cooling, which are more efficient than passive ones but need external driving force such as fans and pumps, increasing the system complexity. Passive cooling methods include fins, heat pipes, PCM and potting materials, which are of simple structures and always used as auxiliary methods due to their relatively low cooling efficiency. The most commonly employed and effective method is the hybrid one, which means the combination of two or more cooling methods (active-active methods, active-passive methods and passive-passive methods).

Each of these methods can be subdivided into various forms according to specific situations. Improved forms in this article are simply summarized as follows:

Forced air cooling: change the structure or number of fans; etc.

Liquid cooling: change the configurations or number of water jacket channels; oil spray cooling; oil immersion cooling; water-oil composite cooling; change the liquid flow rate; etc.

Hybrid cooling: forced air/liquid cooling + fins/HPs/PCM/potting materials; liquid cooling + forced air cooling; etc.

Liquid cooling has the best cooling effect among these methods, especially water cooling. By contrast, advantages of water-cooling lie in its efficient heat dissipation, making it apt for scenarios requiring high power and high speed; and its disadvantages are complex structure, high cost, and tedious maintenance. Advantages of oil cooling are safety, stability, compact structure, and low cost; and its disadvantages are that the heat dissipation performance is relatively weak and not suitable for extreme power requirements.

The development of cooling methods needs balancing multiple requirements such as heat dissipation efficiency, system light-weighting, cost control, and environmental adaptability. So, in the future, cooling methods can be improved in the following directions:

1) Artificial intelligent control system: predicting motor temperature through neural network prediction model; optimization of cooling strategy for connected vehicle big data; etc.

2) Innovation of materials: developing new PCM or potting materials with high thermal conductivity; etc.

3) Integration and innovation between systems: motor-battery thermal management collaboration to improve waste heat utilization efficiency; etc.

All in all, thermal management of an EV motor counts for a great deal due to its foundation of the motor performance, the key defense line for EV safety and the balance pivot between economy and sustainability. Hence, continued efforts are in need for development of cooling methods.

Appendix Summary of cooling schemes

Author	Motor Type	Basis Motor Parameters	Cooling Method	Cooling Object	Research Method	Thesis Title
Ustun et al.	BLDC	70kW	Liquid cooling	Stator	FEA + CFD + Experiment	Design and manufacture of electric powertrain and its cooling system for ITU EV project
Li et al.	PMSM	Average phase current: 474.1A Average torque: 118.8N·m Speed: 22000rpm	Liquid cooling (oil-water composite)	Housing	FEA	Design of Cooling Channel for Stator Immersion Oil Cooled Motor

Author	Motor Type	Basis Motor Parameters	Cooling Method	Cooling Object	Research Method	Thesis Title
Towhidi et al.	IM	11kW	Liquid cooling (housing jacket cooling)	Stator winding	LPTN	Thermal Modelling of an Induction Motor with Liquid Cooling Optimization for Different EV Drive Cycles
Nakahama et al.	BLDC	20kW	Forced air cooling (open type)	Stator end winding	CFD + Experiment	Cooling airflow in unidirectional ventilated open-type motor for electric vehicles
Xu et al.	IM	600kW	Forced air cooling (open type)	Stator winding + Stator core + Rotor core	Multi-physics coupling analysis + Experiment	Thermal Management of Open Air-cooled Induction Motor for Drilling
Xu et al.	IM	600kW	Forced air cooling (open type)	Stator winding	FEA + Experiment	Cooling Enhancement of an Axially Forced Air-Cooled Motors Using Axial Air Deflector
Mizuno et al.	IM	160kW	Forced air cooling (closed type) + Fins	Interior of the motor	Numerical simulation + Experiment	Development of a Totally Enclosed Fan-Cooled Traction Motor
Kim et al.	IM	100kW	Forced air cooling (open type) + Fins	Winding surface	CFD	Effect of air-gap fans on cooling of windings in a large-capacity, high-speed induction motor
Satrústegui et al.	IM	IC71W	Liquid cooling (water jacket cooling)	Housing	CFD + LPTN + Experiment	Design criteria for water cooled systems of induction machines
Zhang et al.	PMSM	40kW	Liquid cooling (water jacket cooling)	Housing + PM	CFD	Energy System Modeling of Liquid Cooled Propulsion Permanent Magnet Synchronous Motor for Electric Vehicles
Park et al.	PMSM	Current density: 20/30/40mm^{-2}	Liquid cooling (oil-water; WJC/ETC/CHC/DSC)	Stator + Coil	CFD	Enhancement of cooling performance in traction motors of electric vehicle using direct slot cooling method
Ye et al.	PMSM	3200rpm-10N·m 1900rpm-400N·m	Liquid cooling (water jacket cooling + oil spray cooling)	Stator end winding	Experiment	Experimental investigation on heat transfer of directly-oil-cooled permanent magnet motor
Deriszadeh et al.	IM	120kW	Liquid cooling (hollow shaft cooling)	rotor	CFD	Model based design and optimization of a shaft cooling for automotive electric motor
Liu et al.	PMSM	150kW	Liquid cooling (housing oil cooling/housing oil cooling+oil spray cooling/housing oil cooling+hollow shaft oil cooling)	PM + Stator winding	Numerical analysis	Effects of cooling methods and key parameters on the cooling performance of oil-cooling motor with hairpin windings
Sibi et al.	BLDC	1kW	Forced air cooling + Fins	Housing + Stator end winding	CFD + Experiment	Cfd simulation on cooling system of electric vehicle bldc motor
Pronin et al.	PMSM	-	Fins	PM + Stator winding	CFD	Principle of Air Cooling of Permanent Magnet Axial Electric Machine
Chai et al.	PMSM	150kW (at max. power/torque)	Heat Pipes	Stator winding	CFD + Experiment	Design and Analysis of High Torque Density Permanent Magnet Synchronous Motor Based on Heat Pipe
Geng et al.	PMSM	Torque density: 7.68N·m/kg	Liquid cooling (water jacket cooling) + Heat Pipes	Stator winding	FEA	Design of Cooling System for High Torque Density Permanent Magnet Synchronous Motor Based on Heat Pipe

Author	Motor Type	Basis Motor Parameters	Cooling Method	Cooling Object	Research Method	Thesis Title
Gu et al.	PMSM	35kW	Forced air cooling + Heat Pipes	Stator winding	FEA + Experiment	Cooling Optimization and Analysis of Air-cooled Axial Flux Permanent Magnet Motors Based on Direct Heat Dissipation with Auxiliary Heat Pipes
Li et al.	PMSM	Rated torque: 1N·m Rated speed: 100rpm	PCM-copper foam composite	Stator winding	FEA + CFD + Experiment	Cooling structure design for an outer-rotor permanent magnet motor based on phase change material
Wang et al.	PMSM	2.53kW	Fins + PCM (paraffin)	Casing	Numerical analysis	Temperature control of permanent-magnet synchronous motor using phase change material
Zhang et al.	Robotic Joint Torque Motor	Rated torque: 2.8N·m Rated speed: 1000rpm	PCM (paraffin)	Casing	Numerical analysis	The Study of Phase Change Thermal Management Schemes for Motors Under Frequent Overloads
Nategh et al.	PMSM	-	Potting material (resin)	Stator winding	Numerical simulation	Thermal and Manufacturing Aspects of Traction Motors Potting: A Deep Experimental Evaluation
Kim et al.	PMSM	16.7kW	Hybrid cooling (housing jacket cooling + rotor shaft cooling)	Rotor + Coil	Numerical analysis + Experiment	Development of an interior permanent magnet motor through rotor cooling for electric vehicles
Huang et al.	PMSM	85kW	Hybrid cooling (forced air cooling + liquid cooling + heat pipes + fins)	Stator	Numerical simulation	A Hybrid Electric Vehicle Motor Cooling System-Design, Model, and Control
Yuan et al.	PMSM	15kW	Hybrid cooling (fins + heat pipes	Stator + Coil	Numerical simulation + Experiment	Thermal management integrated with three-dimensional heat pipes for air-cooled permanent magnet synchronous motor

REFERENCES

[1] C. C. Onn, N. S. Mohd, C. W. Yuen, S. C. Loo, S. Koting, A. F. A. Rashid, M. R. Karim, S. Yusoff, Transp. Res. D Transp. Environ. 2018, 64, 15.

[2] Zeng J, Sun X, Qian Z. Thermal simulation of an oil-cooled permanent magnet synchronous motor[C]/2017 IEEE International Electric Machines and Drives Conference (IEMDC). IEEE, 2017.DOI:10.1109/IEMDC.2017.8001872.

[3] M. Michel, K. Mikhaeel, W. De Bruijn, M. M. K. Mikhaeel, Renew. Sustain. Energy Rev. 2024, 192, 114171.

[4] Ahmad H, Dhamodharan P, Kim S C. Advances in Cooling Technologies for Electric Vehicle Drive Motors, Reducers, and Inverters: A Comprehensive Review[J]. Energy Technology, 2401691.

[5] S. V. K. Akundi, T. W. Simpson, P. M. Reed, in Proc. of the ASME Int. Design Engineering Technical Conf. and Computers and Information in Engineering Conf.–The American Society of Mechanical Engineers, California, USA, DETC2005 2008, 2B, 999.

[6] A. M. Lulhe and T. N. Date, "A technology review paper for drives used in electrical vehicle (EV) & hybrid electrical vehicles (HEV)," 2015 International Conference on Control, Instrumentation, Communication and Computational Technologies (ICCICCT), Kumaracoil, India, 2015, pp. 632-636, doi: 10.1109/ICCICCT.2015.7475355.

[7] R. Saidur, A review on electrical motors energy use and energy savings, Renewable and Sustainable Energy Reviews, Volume 14, Issue 3, 2010, Pages 877-898, ISSN 1364-0321, https://doi.org/10.1016/j.rser.2009.10.018.

[8] R. Wrobel, D. E. Salt, A. Griffo, N. Simpson, P. H. Mellor, IEEE Trans. Ind. Electron. 2014, 61, 4412.

[9] Ahmad H, Dhamodharan P, Kim S C. Advances in Cooling Technologies for Electric Vehicle Drive Motors, Reducers, and Inverters: A Comprehensive Review[J]. Energy Technology, 2401691.

[10] J. Juergens, B. Ponick, O. Winter, A. Fricasse, in Proc. – 2015 IEEE Int. Electric Machines and Drives Conf., IEMDC 2015 2016, pp. 1254–1259, https://doi.org/10.1109/IEMDC.2015.7409222.

[11] S. -Y. Im, T. -G. Lee, K. -W. Kim, J. -C. Park, J. -W. Chin and M. -S. Lim, "Thermal Modeling With Surrogate Model-Based Optimization of Direct Oil Cooling Heat Transfer Coefficient for HEV Motor," in IEEE Transactions on Industry Applications, vol. 60, no. 1, pp. 332-342, Jan.-Feb. 2024, doi:

10.1109/TIA.2023.3314004.
[12] Y. Qin, *et al.*, Renewable Sustainable Energy Rev. 2020, 124, 109782.
[13] Bourgault, A., Taqavi, O., Li, Z., Byczynski, G., & Kar, N. C. (2024). Advanced lumped parameter thermal network for modeling of cooling solutions in electric vehicle motor applications. IEEE Transactions on Magnetics (11), 60.
[14] Bourgault, A., Taqavi, O., Li, Z., Byczynski, G., & Kar, N. C. (2024). Advanced Lumped Parameter Thermal Network for Modeling of Cooling Solutions in Electric Vehicle Motor Applications. 2024 IEEE International Magnetic Conference - Short Papers, INTERMAG Short Papers 2024 - Proceedings. https://doi.org/10.1109/INTERMAGShortPapers61879.2024.10576778
[15] Sibi, S. R., Khaja Najumudeen, A., & Rajeshkanna, R. (2021). Cfd simulation on cooling system of electric vehicle bldc motor. Proceedings of the 7th International Conference on Electrical Energy Systems, ICEES 2021, 117–122. https://doi.org/10.1109/ICEES51510.2021.9383730
[16] O. Ustun *et al.*, "Design and manufacture of electric powertrain and its cooling system for ITU EV project," 2014 International Conference on Electrical Machines (ICEM), Berlin, Germany, 2014, pp. 730-735, doi: 10.1109/ICELMACH.2014.6960262.
[17] Li, Y., Li, Q., Fan, T., Wen, X., & Sun, C. (2023). Design of Cooling Channel for Stator Immersion Oil Cooled Motor. 2023 2nd Asia Power and Electrical Technology Conference, APET 2023, 420–423. https://doi.org/10.1109/APET59977.2023.10489250
[18] Towhidi, M., Ahmed, F., Mollaeian, A., & Kar, N. C. (2020). Thermal Modelling of an Induction Motor with Liquid Cooling Optimization for Different EV Drive Cycles. 2020 10th International Electric Drives Production Conference, EDPC 2020 - Proceedings, 2020-January. https://doi.org/10.1109/EDPC51184.2020.9718577
[19] Nakahama, T., Suzuki, K., Hashidume, S., Ishihashi, F., & Hirata, M. (2006). Cooling airflow in unidirectional ventilated open-type motor for electric vehicles. IEEE Transactions on Energy Conversion, 21(3), 645–651. https://doi.org/10.1109/TEC.2006.877364
[20] Xu, Z., Xu, Y., Ai, M., Liu, W., & Wang, Y. (2021, December). Thermal Management of Open Air-cooled Induction Motor for Drilling. In 2021 IEEE 4th Student Conference on Electric Machines and Systems (SCEMS) (pp. 1-6). IEEE.
[21] Xu, Z., Xu, Y., Wang, Y., & Wang, Y. (2024). Cooling Enhancement of an Axially Forced Air-Cooled Motors Using Axial Air Deflector. IEEE Transactions on Applied Superconductivity, 34(8), 1–5. https://doi.org/10.1109/TASC.2024.3468073
[22] Mizuno,S,Noda,et al.Development of a Totally Enclosed Fan-Cooled Traction Motor[J]. IEEE Transactions on Industry Applications, 2013, 49(4): 1508-1514.DOI:10.1109/TIA.2013.2256872.
[23] Kim, C., Lee, K. S., & Yook, S. J. (2016). Effect of air-gap fans on cooling of windings in a large-capacity, high-speed induction motor. Applied Thermal Engineering, 100, 658–667. https://doi.org/10.1016/j.applthermaleng.2016.02.077
[24] Zi-Chao, Z., Qiang, S., & Ahmed, B. (2019). Innovative Design of the Cooling Topologies for Electric Vehicle Motors. IOP Conference Series: Materials Science and Engineering, 533(1). https://doi.org/10.1088/1757-899X/533/1/012021
[25] Satrústegui, M., Martinez-Iturralde, M., Ramos, J. C., Gonzalez, P., Astarbe, G., & Elosegui, I. (2017). Design criteria for water cooled systems of induction machines. Applied Thermal Engineering, 114, 1018–1028. https://doi.org/10.1016/j.applthermaleng.2016.12.031
[26] Zhang, Z., Song, Q., & Ahmed, B. (2023). Energy System Modeling of Liquid Cooled Propulsion Permanent Magnet Synchronous Motor for Electric Vehicles. 2023 13th International Conference on Power and Energy Systems, ICPES 2023, 424–429. https://doi.org/10.1109/ICPES59999.2023.10400158
[27] Park, J., An, J., Han, K., Choi, H. S., & Seouk Park, I. (2022). Enhancement of cooling performance in traction motor of electric vehicle using direct slot cooling method. Applied Thermal Engineering, 217. https://doi.org/10.1016/j.applthermaleng.2022.119082
[28] Ye, Li, *et al.* "Experimental investigation on heat transfer of directly-oil-cooled permanent magnet motor." 2016 19th International Conference on Electrical Machines and Systems (ICEMS). IEEE, 2016.
[29] Ghahfarokhi, P. S., Podgornovs, A., Kallaste, A., Vaimann, T., Belahcen, A., & Cardoso, A. J. M. (2021, January 27). Oil Spray Cooling with Hairpin Windings in High-Performance Electric Vehicle Motors. 2021 28th International Workshop on Electric Drives: Improving Reliability of Electric Drives, IWED 2021 - Proceedings. https://doi.org/10.1109/IWED52055.2021.9376390
[30] Deriszadeh, A., di Battista, D., di Giovine, G., & Cipollone, R. (2024). Model based design and optimization of

a shaft cooling for automotive electric motor. Journal of Physics: Conference Series, 2893(1). https://doi.org/10.1088/1742-6596/2893/1/012124

[31] Liu, Y. X., Wu, H., Zhang, J., Xu, P. X., Chen, S., He, X. H., & Sun, Z. D. (2024). Effects of cooling methods and key parameters on the cooling performance of oil-cooling motors with hairpin windings. Archives of Thermodynamics, 45(2), 301–309. https://doi.org/10.24425/ather.2024.150874

[32] Y. Quérel *et al.*, "Evaluation of an evaporative cooling solution for hybrid and electrical vehicles motors," 2018 IEEE International Conference on Industrial Technology (ICIT), Lyon, France, 2018, pp. 395-400, doi: 10.1109/ICIT.2018.8352210.

[33] Grabowski, M., Urbaniec, K., Wernik, J., & Wołosz, K. J. (2016). Numerical simulation and experimental verification of heat transfer from a finned housing of an electric motor. Energy Conversion and Management, 125, 91–96. https://doi.org/10.1016/j.enconman.2016.05.038

[34] Sibi, S. R., Khaja Najumudeen, A., & Rajeshkanna, R. (2021). Cfd simulation on cooling system of electric vehicle bldc motor. Proceedings of the 7th International Conference on Electrical Energy Systems, ICEES 2021, 117–122. https://doi.org/10.1109/ICEES51510.2021.9383730

[35] Pronin, E. A., Zharkov, E. O., & Zherebtsov, A. A. (2023). Principle of Air Cooling of Permanent Magnet Axial Electric Machine. Proceedings - 2023 Russian Workshop on Power Engineering and Automation of Metallurgy Industry: Research and Practice, PEAMI 2023, 65–71. https://doi.org/10.1109/PEAMI58441.2023.10299909

[36] R. Geng, G. Liu, T. Mei, Q. Yue and F. Zhang, "Design of Cooling System for High Torque Density Permanent Magnet Synchronous Motor Based on Heat Pipe," 2023 IEEE 6th Student Conference on Electric Machines and Systems (SCEMS), HuZhou, China, 2023, pp.1-5, doi: 10.1109/SCEMS60579.2023.10379406.

[37] Chai, F., Cao, Y., & Pei, Y. (2022). Design and Analysis of High Torque Density Permanent Magnet Synchronous Motor Based on Heat Pipe. 2022 International Conference on Electrical Machines and Systems, ICEMS 2022. https://doi.org/10.1109/ICEMS56177.2022.9982948

[38] Geng, R., Liu, G., Mei, T., Yue, Q., & Zhang, F. (2023). Design of Cooling System for High Torque Density Permanent Magnet Synchronous Motor Based on Heat Pipe. IEEE Student Conference on Electric Machines and Systems (SCEMS). https://doi.org/10.1109/SCEMS60579.2023.10379406

[39] Gu, Y., Li, X., Geng, W., & Zhang, Y. (2024). Cooling Optimization and Analysis of Air-cooled Axial Flux Permanent Magnet Motors Based on Direct Heat Dissipation with Auxiliary Heat Pipes. 2024 IEEE Transportation Electrification Conference and Expo, Asia-Pacific, ITEC Asia-Pacific 2024, 361–367. https://doi.org/10.1109/ITECAsia-Pacific63159.2024.10738551

[40] Biswas K, Abhari R. Low-cost phase change material as an energy storage medium in building envelopes: experimental and numerical analyses. Energy Convers Manage 2014; 88:1020–31.

[41] S. Wang *et al.*, "Temperature control of permanent-magnet synchronous motor using phase change material," 2015 IEEE International Conference on Advanced Intelligent Mechatronics (AIM), Busan, Korea (South), 2015, pp. 1635-1640, doi: 10.1109/AIM.2015.7222778.

[42] Zhang, H., Qiu, S., Wang, J., Chen, J., Sun, X., & Zhang, C. (2024). The Study of Phase Change Thermal Management Schemes for Motors Under Frequent Overloads. 2024 IEEE International Conference on Electrical Energy Conversion Systems and Control, IEECSC 2024, 6–10. https://doi.org/10.1109/IEECSC62814.2024.10913570

[43] S. Nategh, A. Krings, O. Wallmark and M. Leksell, "Evaluation of Impregnation Materials for Thermal Management of Liquid-Cooled Electric Machines," in IEEE Transactions on Industrial Electronics, vol. 61, no. 11, pp. 5956-5965, Nov. 2014.

[44] H. Li, K. W. Klontz, V. E. Ferrell and D. Barber, "Thermal Models and Electrical Machine Performance Improvement Using Encapsulation Material," in IEEE Transactions on Industry Applications, vol. 53, no.2, pp. 1063-1069, March-April 2017.

[45] S. Nategh, "Thermal analysis and management of high-performance electrical machines," Ph.D. Dissertation, KTH Royal Institute of Technology, Stockholm, Sweden, June 2013.

[46] Nategh, S., Boglietti, A., Barber, D., Liu, Y., & Brammer, R. (2020). Thermal and Manufacturing Aspects of Traction Motors Potting: A Deep Experimental Evaluation. IEEE Transactions on Energy Conversion, 35(2), 1026–1035. https://doi.org/10.1109/TEC.2020.2966606

[47] Kea-Ho Lee, Hyun-Rok Cha, Young-Bae Kim, Development of an interior permanent magnet motor through rotor cooling for electric vehicles, Applied Thermal Engineering, Volume 95, 2016, Pages 348-356, ISSN 1359-4311, https://doi.org/10.1016/j.applthermaleng.2015.11.022.

[48] Huang, J., Shoai Naini, S., Miller, R., Rizzo, D., Sebeck, K., Shurin, S., & Wagner, J. (2019). A Hybrid Electric

Vehicle Motor Cooling System-Design, Model, and Control. IEEE Transactions on Vehicular Technology, 68(5), 4467–4478. https://doi.org/10.1109/TVT.2019.2902135

[49] Fang, G., Yuan, W., Yan, Z., Sun, Y., & Tang, Y. (2019). Thermal management integrated with three-dimensional heat pipes for air-cooled permanent magnet synchronous motor. Applied Thermal Engineering, 152, 594–604. https://doi.org/10.1016/j.applthermaleng.2019.02.120